energies

MDPI

Review

Low-Temperature Applications of Phase Change Materials for Energy Storage: A Descriptive Review

Jesus Fernando Hinojosa *, Saul Fernando Moreno and Victor Manuel Maytorena

Deparment of Chemical Engineering and Metallurgy, Universidad de Sonora (UNISON), Blvd. Luis Encinas y Rosales, Hermosillo CP 83000, Mexico

* Correspondence: fhinojosa@iq.uson.mx

Abstract: Thermal storage is very relevant for technologies that make thermal use of solar energy, as well as energy savings in buildings. Phase change materials (PCMs) are positioned as an attractive alternative to storing thermal energy. This review provides an extensive and comprehensive overview of recent investigations on integrating PCMs in the following low-temperature applications: building envelopes, passive systems in buildings, solar collectors, solar photovoltaic systems, and solar desalination systems. Moreover, techniques for improving heat transfer in PCM systems are described. All applications studies indicate that all applications improve their performance when applying a PCM. One of the most beneficiated technologies is the combined PV-Thermal systems (PVT), where some authors reported an increase in overall efficiency greater than 40%.

Keywords: phase change material; buildings; solar energy; photovoltaic; solar desalination; heat exchangers; enhanced PCM; review

Citation: Hinojosa, J.F.; Moreno, S.F.; Maytorena, V.M. Low-Temperature Applications of Phase Change Materials for Energy Storage: A Descriptive Review. *Energies* **2023**, *16*, 3078. https://doi.org/10.3390/en16073078

Academic Editors: Emiliano Borri, Gabriel Zsembinszki and Marilena De Simone

Received: 3 March 2023
Revised: 24 March 2023
Accepted: 27 March 2023
Published: 28 March 2023

1. Introduction

World energy demand grows as the global population increases. The use of renewable energy has been necessary to cater to this demand and to achieve the seventh Sustainable Development Goal, set up in 2015 by the United Nations General Assembly [1].

The primary renewable energy sources are solar, wind, hydropower, biomass, and tidal. The sun provides all the energy that humanity needs in one hour for one year [2]. Therefore, solar energy is far more abundant than any other energy resource on earth, whether renewable or non-renewable, but it has the disadvantage of being intermittent. In order to address this intermittence, using thermal energy storage has been proposed.

The thermal energy storage strategies may be classified into three major groups. They are (a) sensible heat storage, (b) thermochemical heat storage, and (c) latent heat storage. Sensible heat storage is the simplest way to store energy. It consists of a material whose temperature increases/decreases in the energy absorption/release process. Typical materials to store sensible heat are solids such as sand, ceramic, graphene, rocks, and concrete and fluids such as water, oils, and molten salts [3]. The amount of energy stored is determined by the specific heat capacity of the material, the variation in temperature, and the amount of material. Thermochemical storage uses reversible chemical reactions to store energy. An endothermic reaction charges the storage unit; later, an exothermic reaction discharges it. Latent heat storage is the result of the phase change phenomenon. This kind of storage has a more significant energy storage density than sensible heat storage [4]. Since this review focuses on latent heat energy storage, the materials to achieve this storage will be described next.

In thermodynamics, phase change is the transition from one state of matter (solid, liquid, gas, and plasma) to another. The fundamental transitions for each state are shown in Figure 1. The phase change occurs when sufficient energy is supplied/lost by the system. In Figure 1, the phase transitions that require energy are in red, while those that release energy are in blue.

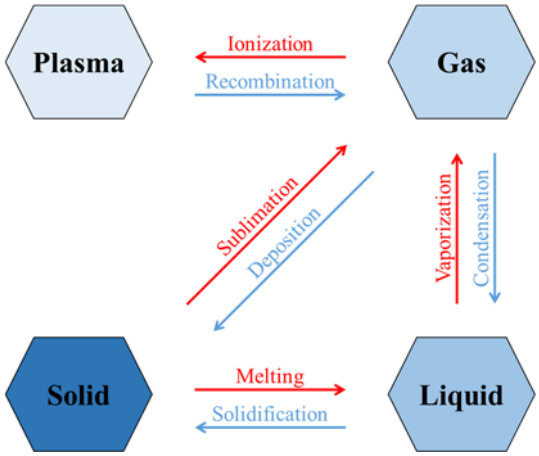

Figure 1. Phase change transitions.

Scientists have shown particular interest in storing thermal energy in the phase change between solid and liquid. This phase change exhibits certain advantages, such as favorable phase equilibrium, high density, minor volume changes during phase transition, and low vapor pressure at the operation temperature [5].

Javadi et al. [6] reported that the most implemented PCMs are paraffin waxes, salt hydrates, fatty acids, and eutectic organic/non-organic compounds. These PCMs are classified into three major groups: organic, inorganic (salt hydrates and metallic), and eutectic. The three groups of PCMs have advantages and disadvantages regarding their thermophysical properties. However, organic materials melt congruently without phase separation but have low thermal conductivity. However, it has been observed that paraffin wax is the most widely used organic PCM due to its narrow melting temperature range, which ranges from −10 °C to 67 °C. These results are consistent with the information found in this document, where it was observed that paraffin wax is the most implemented under different applications and technologies (Figures 8b, 10b, and 13a).

On the other hand, inorganic materials stand out for conserving their thermophysical properties when subjected to many thermal cycles and having a much higher thermal conductivity than organic PCMs and a high volumetric latent heat density (~350 MJ/m^3). However, the main disadvantages of these PCMs are the corrosiveness of the salts on metals, the subcooling condition, and phase segregation. Finally, eutectic PCMs have a defined melting/freezing point and no component separation during phase changes.

The most important parameter for selecting a PCM for a specific application is its melting point, because if the melting point does not coincide with the operating temperature range of the particular application, the phase change phenomenon will not occur. Other relevant parameters are the heat of fusion, thermal and chemical stability, low phase change expansion and contraction, and nontoxicity. Moreover, its availability and low cost are essential criteria for selecting an adequate PCM.

However, the use of phase change materials (PCMs) is broad. Still, the literature survey shows the absence of a comprehensive review of recent studies of PCMs in low-temperature applications (see Figure 2). Therefore, the objective of this review is to provide an extensive overview of recent research advances in the applications of PCMS in the following thermal applications: (1) building envelopes, (2) passive systems in buildings, (3) solar collectors, (4) solar photovoltaic systems, (5) solar desalination systems, and (6) techniques for improving heat transfer in PCM systems. The following sections describe and discuss the main research contributions of recent years, together with the main challenges and limitations detected.

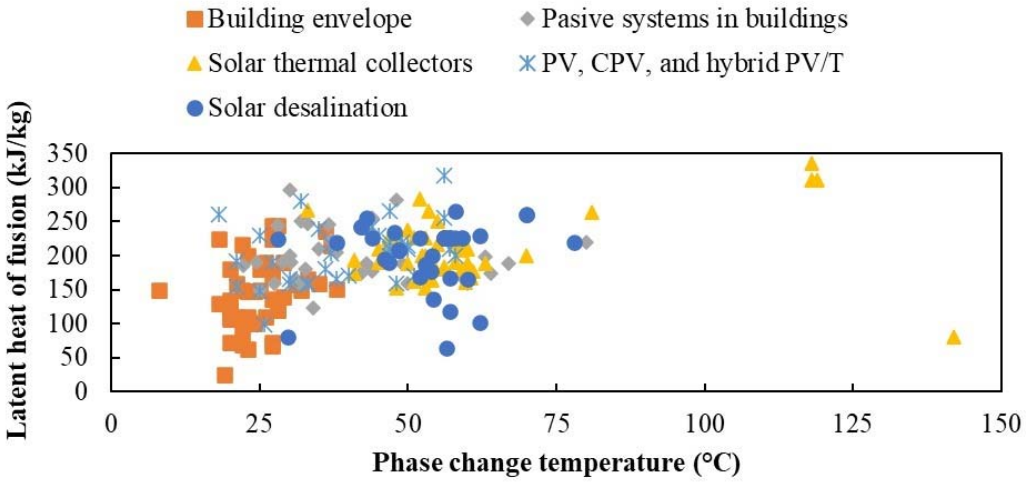

Figure 2. Phase change temperature and latent heat of fusion in low-temperature applications reported in the literature.

2. Use of PCMs in Building Envelopes

A nearly zero-energy building is defined as a building with very high energy performance. Renewable sources should extensively cover the almost zero or very low amount of energy required produced on-site or nearby [7]. One strategy to achieve this is by decreasing space heating and cooling energy through an energy-efficient building envelope [8]. On the other hand, it is known that energy storage reduces energy consumption in buildings [9].

PCMs are often used to mitigate and time-shift thermal load peaks. They gain heat (charge) during warmer daytime via melting and solidification due to releasing energy (discharge) during cooler nighttime. Therefore, PCMs may increase energy efficiency when integrated into a building's envelope. The primary usage of PCMs in a building envelope is shown in Figure 3. The PCM is placed in building walls (Figure 3a) or top roofs (Figure 3b), combined with building material and thermal insulation. Next, recent studies of PCMs in the building envelope are described.

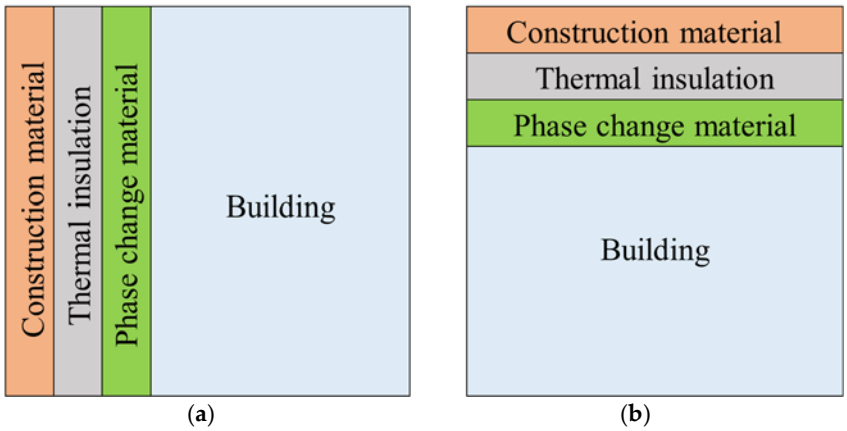

Figure 3. Basic usage of PCMs in building envelope in (**a**) walls and (**b**) roof.

Guichard et al. [10] set up an actual building equipped with PCMs on a complex roof and presented a mathematical model based on the effective heat capacity. They placed a 5.26 mm PCM slab on the roof. The PCM had a melting temperature of 23.4 °C. The results they presented were based entirely on the predictive capacity of the mathematical model. Liu et al. [11] proposed a polyvinyl acetate-based wall tile with PCM inside to enhance the thermal performance of exterior walls. They used capsules composed of octadecane (80%) and wall material (20%), with nominal latent heat and a melting point of 180 J/g and 28 °C, respectively. They found that the proposed system can reduce the peak heat flux by at

least 70% and up to 80%. Chung and Park [12] studied how well plates with phase change materials (PCMs) worked at managing temperature, using two PCMs that melt at different temperatures (25 and 44 °C) and with two different levels of reflectivity. They found that the PCM with a melting temperature of 44 °C kept the surface and inside temperatures lower than the PCM with a melting temperature of 25 °C. Mazzeo et al. [13] developed a methodology to be applied to layers of different PCMs and performed under different climatic conditions (Continental and Mediterranean conditions) in two locations. The PCM melting temperatures range from 15 to 32 °C. Highlighted for both sites, the yearly energy stored had its highest value with a melting point of 23 °C. On the other hand, for the winter season, the lower the melting, the better, contrary to the summer season.

Reddy et al. [14] studied the thermal behavior of roofs with PCMs. The analysis showed that with several layers of PCM (melting temperature of 29 °C), it was possible to maintain a temperature of about 28 °C in the building. Moreover, there was a reduction in heat gain by 25 to 36% compared to the roof without the PCM layer. Zhou et al. [15] experimentally studied the heat absorption/release performance and the impact on indoor heat gain of a roof module made of microencapsulated PCM inside an aluminum honeycomb board. They tried two PCMs with melting points of 37 and 43 °C. Their results indicated that the roof module with a 37 °C melting temperature had improved peak load-shifting capacity but had a slightly increased indoor heat gain. The PCM was cooled entirely at night in both roof modules to begin a new thermal cycle the next day. Bendic and Dobrotă [16] analyzed (theoretically and experimentally) an intelligent composite material with PCM for constructing a dwelling. They made a micro-encapsulation and added those capsules inside a wall. The maximum room temperature of 4 °C was reduced by reducing the heating load at night. The utilized PCM was butyl stearate, which has a melting/solidification temperature of around 19 °C. Rashid et al. [17] compared sandwich concrete blocks with different insulation materials, such as PCMs and waste materials. They used two PCMs with melting temperatures of 30 and 42 °C. Their findings are that the PCMs produce an energy saving of 45.4 and 43.3% in summer and 31.6 and 28.7% in winter, respectively. There was no significant difference in using PCM or waste material (date palm) in summer, but in winter, waste material (rubber tire) performed better than PCMs.

Ascione et al. [18] optimized the design of an educational building by adding PCM to the inner side of the external walls. The PCM had a melting and freezing point of 23 and 21 °C, respectively. It theoretically reduced the summer energy consumption by 11.7% and increased the summer indoor comfort by 215 h. Moreno et al. [19] numerically and experimentally studied the heat transfer in a cavity filled with air with one vertical wall with a PCM. They studied the effect of the Rayleigh number and PCM thickness on the Nusselt number and the average air temperature. The PCM had a melting temperature of around 29 °C. They noticed that the molten PCM generated a temperature gradient along the vertical direction, which caused an uneven temperature at the shared wall. Tsoka et al. [20] simulated the thermal behavior of a sustainable reconstructed innovate module, which contained PCM. They modeled four different climates in Greece. For all the cases, the annual percentage of the total occupancy time inside the comfort conditions exceeded 56% with a PCM melting point between 24 and 28 °C. Charvátová et al. [21] numerically studied the distribution and time evolution of the temperature in a wooden house in summer with PCM. The phase change temperature of the PCM was 22 °C, and the latent heat was 200 kJ/kg. The maximum temperature decrease was 3.9 °C compared to the house in which the PCM and the house without the PCM coverage covered the wall opposite the window.

Ho et al. [22] studied the effects of the pipe wall properties on the heat transfer performance of a rectangular thermosiphon with a PCM suspension, aiming to ensure the optimum heat transfer efficiency in the cooling section. Rehman et al. [23] investigated a hybrid building envelope built with PCM and local organic waste materials. The PCM was calcium chloride hexahydrate ($CaCl_2 \cdot 6H_2O$) embedded in a brick and corn husk. The maximum indoor temperature was 27 °C when the envelope had 6% corn husk composite material mixed with the PCM. Ye et al. [24] evaluated a building envelope's

thermal performance and energy consumption with phase change energy storage and a ventilated cavity. The effects of placing the PCM on the roof and the walls were tested. They used a composite PCM with magnesium nitrate hexahydrate ($Mg(NO_3)_2 \cdot 6H_2O$) at different concentrations (0, 2, 5, 8, 10, 12, 15 wt%). The melting temperature for different concentrations ranged from 10 to 30 °C. The proposed configuration could save up to 30% of energy compared with the ventilation-free and uncoated Trombe wall. Rehman et al. [25] proposed a novel dual-layer PCM configuration for brick walls to maintain human comfort in hot and cold climatic conditions in Islamabad, Pakistan. The PCMs for this study had a melting temperature of 13 and 29 °C. Brick, PCM, expanded polystyrene, PCM, and brick composed the wall. The results show that combining both PCMs reduced energy requirements for this city throughout the year than using a single PCM (29 °C) for summer or winter (13 °C) alone.

Kavgic et al. [26] simulated four hempcrete and hempcrete–PCM wall design configurations and compared them to reduce energy demand. They took into consideration the hysteresis phenomenon in the PCM. The melting point was between 15 and 23 °C, and the freezing point was between 16 and 7 °C. The hempcrete–PCM wall types outperformed the hempcrete wall assembly by up to 7% for heating and 20.7% for cooling energy savings. Kobeyev et al. [27] used energy simulation tools (OpenStudio and EnergyPlus) to design and analyze the performance of a hotel building in hot and dry climate conditions. They incorporated the building's three sustainable technologies (thermochromic windows, PCMs, and solar panels). The PCM temperature varied from 20 to 30 °C for the selected material. They found the PCM to be economically nonviable, although it reduced energy consumption by 10.03% (222 GJ). Zhou et al. [28] investigated the heat transfer performance through building walls with installed PCMs via an explicit finite element method. They analyzed different wall configurations varying the material sequences and layer thickness of extruded polystyrene and PCM. The selected PCM had a melting point of 28 °C. They concluded that the location of the PCM depends on the requirement of the application.

Baccega and Bottarelli [29] elaborated on a lime-based plaster and its enhancement containing 10% by mass of granular PCM to be applied on a historical building's envelope. The granular PCM had a melting temperature of 28 °C. Significant improvements were observed from using PCM in the plaster, with reductions in the incoming energy between 9% and 18%, compared to a reference lime-based plaster and a lime–plaster reported in the literature, respectively. Cui et al. [30] developed a 3D printed phase-change concrete adding microencapsulated paraffin to a 3D printable material. They made three mixes (0, 10, and 20 wt%). The phase change temperature of the PCM was around 23.6 °C. The material with 20 wt% PCM exhibited a peak temperature reduction of 8 °C. They also concluded that PCMs did not diminish the material buildability and printability. Bruno et al. [31] investigated a temporary housing unit's energy efficiency for the Mediterranean climate. The building's panels were made of cork and bio-PCM, and they tested different Bio-PCM melting temperatures, locations within the walls, and quantities. They found that the Bio-PCM with a melting temperature of 23 °C provided the best results, with monthly electricity savings ranging from 25 to 65%.

Liu et al. [32] evaluated the influence laws and effectiveness of different configurations of PCM on the thermal performance of lightweight building walls in summer and winter. The melting range of the PCMs was between 30–40/22 and 32/14–24 °C. Their 58.2 and 36.4% configuration decreased the peak and average heat flux. Hou et al. [33] investigated how different thermal parameters of PCM affected the annual energy demand and recommended the best combination of parameters. They tested various parameters, including melting temperature ranging from 8 to 24 °C. Their recommended PCM could save 20.7% of annual energy demand. They also discovered that the thickness and conductivity of PCMs were the most sensitive parameters affecting the yearly energy demand. The thickness and density of PCMs were the most sensitive parameters affecting economic benefits. Terhan and Ilegar [34] investigated the effects on the building's thermal energy performance using two different PCMs integrated into the exterior walls at various thicknesses and melting

temperatures. The best thermal energy performance among all external wall types represented 24.45% total energy savings in the cooling season and 14.76% in the heating season. This performance was achieved with a PCM whose melting temperature was 21 °C.

3. Integration of Passive Systems with PCMs in Buildings

The integration of PCMs into the following passive systems in buildings: (1) Trombe wall, (2) solar chimney, (3) earth-to-air heat exchangers, and (4) glazing systems, is presented next.

3.1. Trombe Wall

PCM is integrated into Trombe wall systems for both cooling and heating applications. The primary usage is embedded in the absorber wall, as seen in Figure 4. This integration extends the operation time due to the latent heat energy storage. The PCM produces some benefits when integrated into Trombe walls, such as enhancing thermal performance and indoor thermal comfort, optimizing solar gain utilization, improving thermal mass storage, preventing overheating problems, and saving energy [35]. Next, investigations integrating PCM into Trombe walls are briefly described.

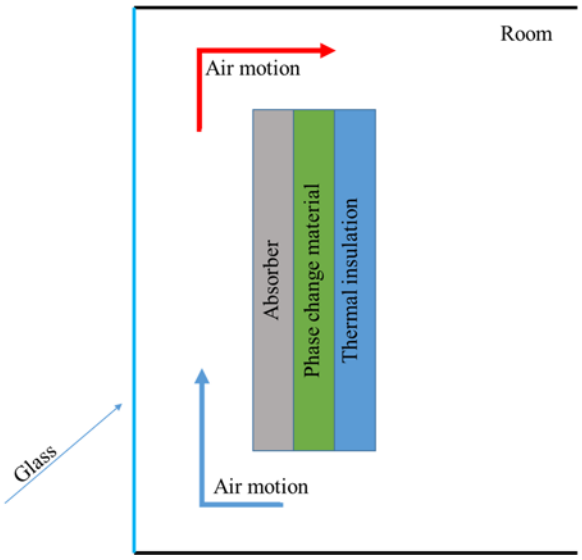

Figure 4. Example of Trombe wall integrated with PCM.

Liu et al. [36] investigated the thermal performances of a system composed of a PCM Trombe wall and a PV/T panel integrated with PCM. The PCM for the Trombe wall and panel had a melting temperature of 22 and 45 °C, respectively. Their optimal parameters were a mass flow rate of 1 kg/s, diameter of water pipe of 0.6 m, temperature of water at the inlet of 15 °C, and thickness of PCM of 20 mm. Tenpierik et al. [37] studied a potential solution for countering the overheating of PCM when utilized in facades (Trombe wall). They segmented the PCM block into three and five separated cavities for a melting point of 25 °C. After that, they placed different PCMs in each cavity, increasing the melting point (23, 24, 25, 27, and 29 °C) with height. This last configuration showed a more uniform melting front. Szyszka et al. [38] experimentally analyzed a system named thermos-diode Trombe wall. It was like the regular Trombe wall but contained large cans with PCM. The PCM melting temperature ranged from 27 to 29 °C. The system generated significant natural convection inside the air cavity, with temperatures higher than 35 °C in the upper section. The ratio of heat flux entering the conditioned space to solar irradiation received reached up to 15.3%.

Leang et al. [39] compared three room configurations (a) no Trombe wall, (b) concrete Trombe wall, and (c) PCM Trombe wall. The melting temperature of the PCM ranged between 25.83 and 27.37 °C. The two Trombe wall systems displayed similar minimizations

of the one-year energy heating demand inside the room (20.45% for concrete and 19.90% for PCM) against the no Trombe wall configuration. Lichołai et al. [40] investigated how glazing parameters affected the thermal performance of a Trombe wall that included a PCM. The PCM had a melting temperature between 22 and 26 °C. Their analysis was not based on the effect of the PCM. However, the PCM's melting time was one criterion for selecting the best glazing.

Kong et al. [41] conducted a comparison study to investigate the thermal performance of the common wall without PCM, the typical single-layer PCM wall, the common double layers PCM Trombe wall, and the new double layers PCM Trombe wall using the validated computational fluid dynamics models. The results showed that the average temperature in the new double-layers PCM Trombe room could be reduced by 0.4–0.93 °C in summer and enhanced by 0.3–6.6 °C in winter. Furthermore, the heat flux can also be reduced by 9.1–92% in summer and 1.8–75.7% in winter. Sheikholeslami and Al-Hussein [42] numerically modeled the transient flow and the heat transfer within a solar system with the Trombe wall. The classic Trombe wall includes three layers (insulation, absorber, and concrete). To boost the efficiency of this solar unit, the PCM layer has been combined as the fourth layer. They involved three positions in their simulations: near the absorber, the middle side, and the insulated wall. They considered the type of PCM RT18 paraffin and a variant to increase the conductivity, and alumina nanoparticles were mixed with base PCM (NPCM). They found that the temperature of the air gap at the right and left sides had been augmented compared to the classic case. Zhou et al. [43] investigated the thermal behavior of a building envelope having a Trombe wall incorporating PCM during the heating season. The results showed that the flow transition and temperature rise mainly happened in the near-wall regions near the room ceiling and the air channel. They also indicated that the Trombe wall with PCM prevents large fluctuations in room temperature and airflow rate.

3.2. Solar Chimney

Solar chimneys are open cavities that induce air movement with the assistance of solar radiation. They can be attached to rooftops or building walls. The integration of the solar chimney with PCM in the building roof is shown in Figure 5. A traditional solar chimney construction material (concrete, brick, and rock) requires a high volume to generate adequate thermal storage. Adding PCM to solar chimneys aims to achieve this thermal storage using less material [44].

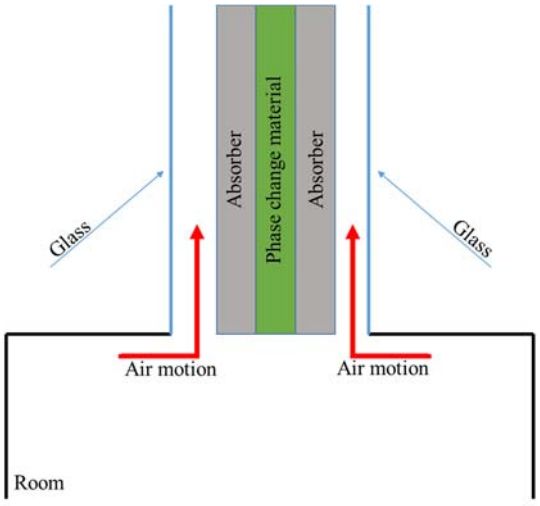

Figure 5. Example of solar roof chimney with PCM.

Thantong et al. [45] experimentally studied the thermal performance of a new configuration of solar chimneys integrating a PCM to enhance natural ventilation and reduce heat gain. The ventilation reduced by 57.2% the heat gain admitted through the south wall. Xamán et al. [46] analyzed the effect of three types of absorbing materials ((1) a lightweight

plate (copper)—reference case, (2) a PCM, the melting temperature of which ranged from 46 to 50 °C, and (3) a heavyweight wall (concrete)) on the heat transfer for a solar chimney. They analyzed three orientations (east, west, and south). The results showed that the solar chimney with a copper plate had the highest mass flow rates and thermal efficiency. The PCM changed its phase to a liquid state in 135 min in the west orientation. Tiji et al. [47] investigated a PCM-enhanced solar chimney, analyzing the effect of adding fins to the absorber plate. The PCM changed its phase between 30 and 34 °C, and the inclination angle of the absorbed plate was set to 60 °C. The results indicated that the PCM enhanced the temperature uniformity inside the room, and the use of fines resulted in a 20% enhancement in the room's mean temperature compared with the non-finned case.

Ashouri and Hakkaki-Fard [48] investigated the effect of using finned absorbers combined with PCM composites on the performance of a solar chimney–PCM–PV system. They tested three PCMs with melting temperatures of 42.76, 50, and 56.75 °C. It improved the ventilation capacity, duration, and power generation, increasing the mass of the PCM for finned cases, contrary to finless cases. They also found that using paraffin inside a copper foam as the PCM resulted in the highest power output and ventilation duration. Li et al. [49] experimentally studied the effects of the inclination angle (30, 45, and 60°) and heat flux (400, 500, and 600 W/m^2) on the performance of a solar chimney with PCM. The obtained results demonstrated that the inclination angle affects the buoyancy effect and the natural convection in the PCM. The maximum outlet air velocity was 0.34 m/s for 60° and 600 W/m^2. Nateghi and Jahangir [50] used EnergyPlus to model a house in three modes: without SC, with SC, and with SC combined with a layer of PCM. For these cases, terms of thermal comfort have been determined under three climates: hot–arid (Yazd), hot–humid (Bandar Abbas), and cold semi-arid (Tehran) climates. The results showed that PCM-assisted solar chimneys provided indoor thermal comfort for hot–humid and cold semi-arid climates, but not for hot–arid climates. They chose to use a different melting point for each season, namely 42 °C for summer, 25 °C for winter, and 35 °C for the whole year.

3.3. Earth-to-Air Heat Exchanger (EAHE)

EAHE is considered an effective heating/cooling technology for buildings. It consists of an array of pipes buried underground at a particular depth. Air flows through these pipes and becomes heated/cooled in winter/summer. The EAHE supplies air to the building at a more comfortable temperature. Figure 6 is a cross-section representation of the EAHE plus PCM system. The basic EAHE only uses sensible heat storage. Meanwhile, EAHE plus PCM uses sensible and latent heat. Moreover, PCM may reduce the soil's thermal saturation, a problem associated with using EAHEs.

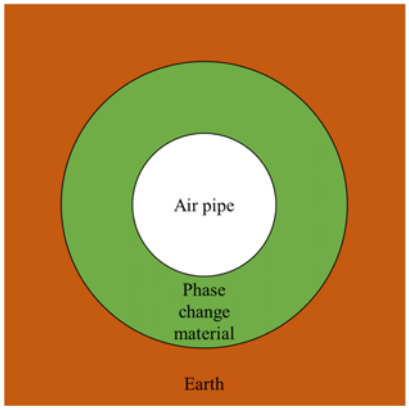

Figure 6. Example of solar earth-to-air heat exchanger (EAHE) integrated with PCM.

Rodrigues and Gillott [51] proposed a novel hybrid space-conditioning system combining EAHEs with PCMs, which uses surfaces as heating or cooling sources to provide better temperature distribution across a space and comfort enhancement with low energy use.

Compared with a reference room, their system could decrease temperature swings by up to 47%. Estrada et al. [52] designed an EAHE based on sensible heat transfer and latent heat exchanges. Zhou et al. [53] compared an EAHE filled with PCM against a traditional one. They complemented the sensible energy storage capacity of the soil with the latent energy storage of the PCM. The PCM phase change temperature ranged from 28 to 32.68 °C. The novel system achieved a maximum outlet temperature of 0.83 °C lower than the traditional one and a 20.24% improvement in cooling capacity. Liu et al. [54] proposed a novel vertical earth-to-air heat exchanger system integrated with annular PCM. They found that the outlet air temperature range decreased with the increase in PCM lengths, while a downward trend in the fluctuation decrease can be observed. In addition, an economic analysis of the proposed system was conducted, indicating that its static payback period was 20.8 years.

Yang et al. [55] studied a cylindrical annulus composed of PCM to regulate the supplied air temperature in ventilated buildings exposed to fluctuating thermal environments. They numerically investigated the effects of the flow rate through the EAHE tube, the melting temperature of the PCM, the external diameter of the EAHE, and the tube length on the EAHE performance. The results demonstrated a maximum reduction in air temperature of 5.4 °C. Zhou et al. [56] proposed a cylindrical PCM-assisted EAHE to improve the performance of such systems. The PCM was in the interior of a concentric pipe, and the air flowed in the annulus section. The daily maximum cooling capacity of the system increased by 28.55–39.74%, the capacity of a conventional one. Additionally, it could dampen fresh air temperature fluctuation to approximately 1 °C. Lu et al. [57] proposed an innovative PCM ceiling coupled with an EAHE cooling system for building cooling. They used a PCM whose melting temperature ranged between 27.4 and 30.2 °C. Their result showed that the experimental room could reduce peak temperature by 2.1 °C under an 8 h timed cold storage strategy and 2.7 °C under a 12 h cold storage strategy. Qin et al. [58] suggested a new integrated system that combines an EAHE with a SAH that includes PCM. Their findings illustrate that implementing PCM could effectively stabilize the outlet air temperature for nearly 4.5 h and prolong the working period to 24 h. Moreover, increased PCM thermal conductivity could improve the system's nocturnal thermal behavior. Qin et al. [59] examined the impact of various factors, including PCM types, PCM structure, and PCM locations, on a new vertical air–soil heat exchanger. Their findings indicated that the RT 20 in the tubular PCM was the most effective option, with the smallest outlet temperature variation. Additionally, the precise placement of the PCM proved to be a viable solution for balancing the daily cooling storage capacity and the outlet temperature variation.

Liu et al. [60] presented a design for an EAHE system assisted by a PCM. The system added PCM in the space between the air pipe and the container walls. The PCM melting temperature was 25 °C. The maximum cooling capacity for the systems was 9.02 kWh. Liu et al. [61] introduced a vertical EAHE system incorporating annular PCM. They conducted a multivariate analysis of various thermo-physical parameters of the PCM to assess their impact on the cooling capacity and the fluctuation of outlet air temperature. They observed that the PCM fusion temperature and latent heat had the most significant influence on the cooling capacity, while the PCM thickness and melting temperature had the most significant impact on temperature fluctuation. Their findings suggested that PCM fusion temperatures between 20 and 22 °C would be ideal. Maytorena et al. [62] proposed using PCM to reduce the soil's thermal saturation and a recovery operation (cool night air injection). They compared two PCMs; their melting temperatures were 35 and 30 °C, respectively. The air temperature in contact with the soil decreased by 2.65 °C with the right PCM. Long et al. [63] developed a new passive system by combining a solar chimney with an earth–air heat exchanger to provide fresh air and cooling passively. To address the mismatch between solar radiation, airflow, and internal load, they integrated a PCM onto the roof of the building. The melting temperature of the PCM ranged from 38 to 43 °C. Their findings indicated that the system with PCM had a maximum absorber surface temperature of 78.8 °C, 16.2% lower than without PCM. The PCM also increased the airflow rate by 50% at night and raised the maximum air temperature by 0.8 °C.

Ouzzane and Bady [64] conducted a theoretical study of a new hybrid system that combines an earth–air heat exchanger (EAHE) as the primary system with a concentric two-pipe heat exchanger as the secondary system. The inner pipe of the secondary system is filled with frozen water or a mixture of ethylene glycol and water as a PCM, and it has longitudinal fins. The air is cooled as it exchanges heat with the frozen PCM in the secondary heat exchanger. Their findings suggest that the proposed system can cool the air by almost 5 °C. Guo et al. [65] conducted a study on a system that combines an EAHE and PCM to provide continuous cooling to indoor spaces. The PCM was integrated into the building envelope to store the excess cold produced by the EAHE at night and release it indoors over time. The PCM had a phase change temperature ranging from 22.2 to 24.4 °C. The system was found to have an average cooling capacity of approximately 1186.5 W. Moreover, the combined operation mode of the EAHE and PCM reduced the time-averaged indoor air temperature by 6.6 °C compared to using only the PCM operation. Maytorena et al. [66] incorporated two passive technologies (a rectangular earth–air heat exchanger assisted with PCM plus a PCM in the room's ceiling) intending to produce thermal comfort conditions in a room exposed to extreme desert climatic conditions. The roof's PCM dropped the ceiling's peak heat flux by up to 33%.

3.4. Glazing Systems

Figure 7 presents a basic scheme of a glazing system with PCM integrated into the middle of two glass panes. It is well known that glazing systems are responsible for an essential part of the thermal loads in rooms or buildings, so using PCM may reduce them.

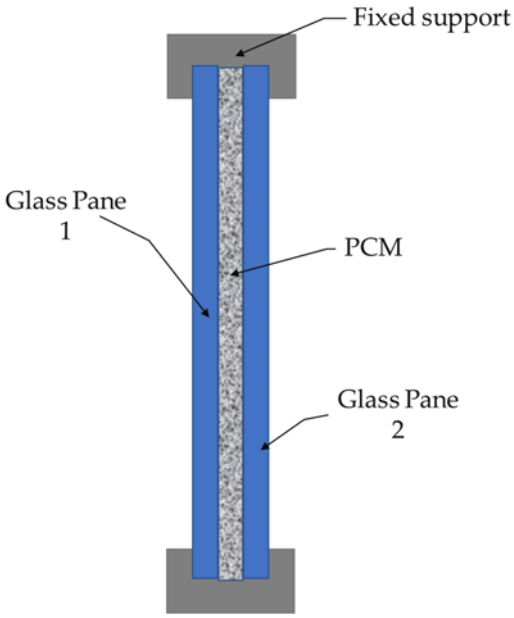

Figure 7. Example of glazing system integrated with PCM.

Durakovic and Torlak [67] conducted an experimental and numerical study of a windows system with a PCM. The authors found that the design of the proposed window could considerably reduce the heat gains by increasing the PCM thickness up to 24 mm. Duraković and Mešetović [68] reported an experimental investigation of PCM glazing systems using a test chamber. It was observed that with the use of PCM, the peak temperatures and average air temperatures were reduced significantly. Zhang et al. [69] investigated the thermal performance of a multiple-glazing roof filled with two PCMs. It was concluded that properly selecting the melting temperature of PCM helps decrease indoor thermal loads in winter and summer. Li et al. [70] reported the energy performance of a roof based on silica aerogel–PCM glazing systems. It was found that the optimal energy performance of the roof occurs with a fill ratio of PCM equal to 80%. Still, when the light transmission

properties are considered, the recommended fill ratio of PCM is 60%. Wang et al. [71] studied a double-glazing unit filled with PCM under fire conditions. It was found that the fire resistance of the unit filled with paraffin wax is better than that of the ordinary unit.

As a summary, the general characteristics of the previously analyzed papers (Sections 2 and 3) are shown in Figure 8. Figure 8a indicates that 47% of the research is experimental, whereas 30% is numerical–experimental and 23% represents numerical investigations. However, Figure 8b shows that 74% of the studies used an organic PCM, 14% used composites, and 12% used inorganic PCMs.

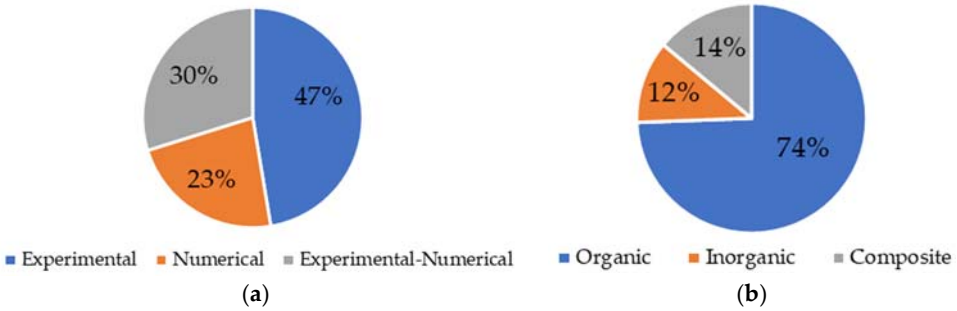

Figure 8. Classification of studies on integrating PCMs in buildings' envelope and passive elements. (**a**) Research approach and (**b**) PCM type.

4. Integration of PCMs in Solar Thermal Collectors

The solar collector is a mature technology used widely worldwide. It can contain heat water or air until about 100 °C. However, PCM integrated (Figure 9) into the solar collector (SC) permits it to increase the thermal efficiency because the PCM absorbs a part of the incoming solar radiation to store thermal energy and extend the operation period of the SC. Figure 10 presents a general classification of selected studies on integrating PCM in solar thermal collectors. It can be observed (Figure 10a) that 33% of papers are theoretical–numerical, whereas 28% are experimental, and 23% are a combination of experimental and theoretical investigation. Moreover, Figure 10b shows that 59% of all research used an organic PCM, 25% a composite PCM, and 16% an inorganic PCM.

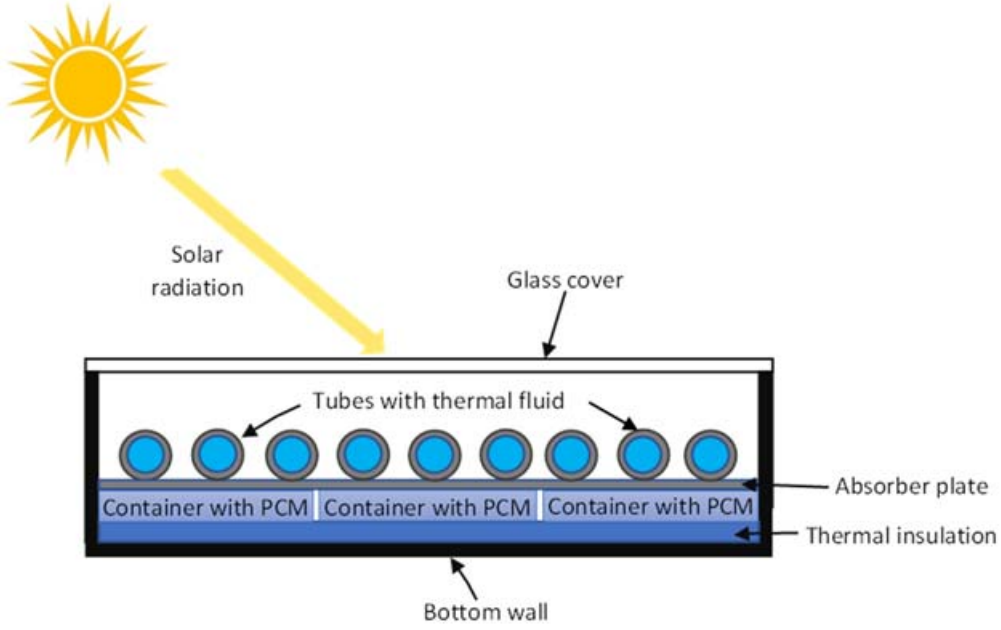

Figure 9. The basic scheme of a solar collector with PCM.

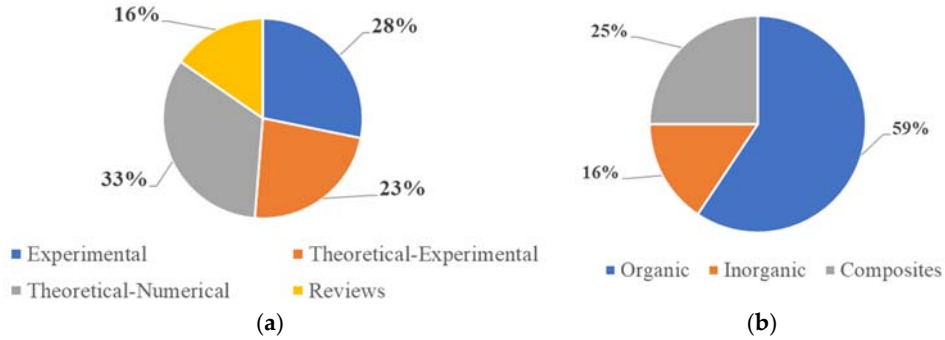

Figure 10. Classification of studies on the integration of PCMs in solar thermal collectors. (**a**) Research approach and (**b**) PCM type.

Wang et al. [72] analyzed the effect of two layers of different PCMs added to a flat plate solar collector (FPSC). One layer had a fusion temperature of 70 °C and another a fusion temperature of 15 °C. It was concluded that the modified SC may solve the phenomenon of overheating and freezing. Abuşka et al. [73] built a solar air collector (SAC) that combined a PCM with an aluminum honeycomb. They investigated the effect of using a honeycomb core on the collector's thermal performance. The experiments tested the heat storage material in two forms: PCM with honeycomb core in the first collector and only PCM in the second collector. Moreover, a third collector with a flat absorber plate was used for comparison. It was concluded that using a honeycomb core as a heat conductivity enhancer material is very functional during the discharge period. Charvat et al. [74] analyzed the influence of PCM coupled with the absorber plate of the SC. Two experimental SACs were built. One SAC used a sheet metal as an absorber plate, while the other made its absorber plate with nine aluminum containers filled with a paraffin-based PCM. A validated model of the solar air collector for the TRNSYS simulation tool was obtained. Palacio et al. [75] reported a comparative experimental analysis of a conventional flat plate solar collector and an identical prototype with a thermal storage system by PCM. Experimental and analytical results indicated that the contact thermal conduction between the absorber surface and PCM and the selection of the PCM itself are critical factors in increasing the collector performance compared to typical flat plate SC. Benkaddour et al. [76] studied a novel hybrid composite PCM/concrete wall integrating a plan solar water heater. The system consisted of a three-layered composite PCM/concrete wall; the middle layer is the paraffin wax PCM. The external interface is directly coupled with a solar water heat absorber. The transmitted heat is transferred to the water, causing a gradual increase in its temperature leading to the maximum benefit of using latent heat storage. Aramesh and Shabani [77] evaluated the evacuated tube solar collector (ETSC) assisted with PCM. They found four different configurations for the coupling of PCMs and ETSC. The advantages and disadvantages of each design were presented.

Chopra et al. [78] analyzed an ETSC with/without PCM. They encountered that ETC/S had higher energy and exergy efficiencies for all selected flow rates than the ETC/WS design. Moreover, the techno-economic analysis indicated that ETC/S's cost of hot water production by ETC/S is lower than ETC/WS's. Javadi et al. [6] reported an extensive overview of the research progress obtained in the field of PCM integrated with solar thermal applications. They concluded that PCM is beneficial in reducing energy consumption, decreasing temperature fluctuation, reducing electricity consumption, and shifting the peak loads of cooling energy demands. Abu-Arabi et al. [79] investigated the behavior of a solar still with glass cooling (SSC), SSC coupled with an SC (SSCC), and SSCC with PCM (SSCCP). Three PCMs were tested. The SSCCP raised the water production up to 2.4 times. Bejan et al. [80] investigated the behavior of transpired solar air collectors (TSCs) with integrated PCMs compared to TSCs without PCMs. The data showed that for the TSCs with PCM, the maximum overall efficiency is improved by almost 6%; the maximum heating capacity is approximately 7.7% higher during the cooling/PCM discharge period,

and the average heating capacity is over five times higher. Ebrahimi et al. [81] evaluated the effect of using PCMs on the thermal performance and overall drying efficiency of an FPSC. The drying time decreased by about 21.87% using PCM at the end section of the FPSC. Depending on the position of the PCM, the thermal efficiency of FPSC increased between 5.02% and 10.13%. Elarem et al. [82] reported a new ETSC incorporating an NPCM with fins. The effect on the system performance of adding copper (Cu) nanoparticles to PCM (paraffin wax) was studied. The results showed that adding fins significantly affects the heat transfer within the PCM. Thakur et al. [83] reported a review of the developments made on flat plate solar collectors (FPSCs) for heat transfer enhancements (HTEs) using PCMs and reflectors. The article discusses the effect of integrating FPSCs with PCM and reflectors for HTEs. It was concluded that PCM acts as thermal storage batteries and escalates the efficiency of FPSCs.

Wheatley and Rubel [84] designed a testing apparatus to investigate the different PCM blends to find the optimum ratios for a highly efficient solar thermal water heating system. Assadeg et al. [85] presented new steady-state energy balance and exergy equations for a novel double-pass solar air collector with fins and PCM. The optimum energy efficiency of the proposed collector is 73% at a mass air rate of 0.15 kg/sec. Zhang et al. [86] built a solar air collector with PCM (SACSU). The thermal conductivity of the PCM was enhanced with expanded graphite (EG) in a mass fraction of 3%. The results showed that the SACSU could extend its operation for almost two hours compared with ETC. Luo et al. [87] developed a thermal model for an air double-pass solar collector with a PCM rod embedded in a vacuum tube. The thermal model was used to analyze the influence of operational parameters and climatic conditions. It was computed that the instantaneous thermal efficiency increased from 13% to 397%. Alshukri et al. [88] reported an experimental investigation for PCM integration in the evacuated tube (ET) and tanks adjacent to the water tank. The new configuration improved the overall solar water heater performance. Nawsud et al. [89] reported a literature review on the potential of NPCM in parabolic trough solar collectors (PTCs). The authors conclude that NPCM and nano-fluids may enhance the mean thermal efficiency in PTCs.

Li et al. [90] analyzed a hybrid photovoltaic and thermal solar energy collector with PCM (PVT–PCM). The thermal system combines air-based and water-based conditions to meet a building's heat demand in different seasons. The PCM was used to absorb the heat the thermal system did not remove. The results showed that the energy-saving efficiency is 64.2%, and the system's additional payback period is 13.1 years. Feng et al. [91] numerically studied a solar evacuated tube collector (ETC) performance using PCMs with a three-dimensional model. The effect of several PCM properties was evaluated. Additionally, the effects of the carbon nanotube mixed in the thermal fluid and the mass flow rate were analyzed. It was concluded that PCM with a latent heat of 160 kJ/kg produces the best performance. Wang et al. [92] evaluated a new type of supercooled PCM in a flat panel solar collector. Experiments verified a computational fluid dynamics (CFD) model. The results showed that the efficiency increased by about 15% when the absorber plate directly interacted with the PCM. Peralta et al. [93] performed a parametric analysis, probing different absorbing materials to find the best configuration that maximizes the energy efficiency of a massive solar–thermal collector. Cementitious materials combined with PCMs with distinct melting (and solidification) temperatures were tested. It was found that the inclusion of PCMs within the absorber material of the collectors can improve the energy performance of these devices.

Palacio et al. [94] presented an experimental analysis of a dual-duct SAC with and without PCM. Two identical prototypes were designed and constructed; one had PCM in the absorber plate. The outlet temperature of the SAH without PCM was consistently 10 °C lower compared to the collector with PCM. The PCM maintained the heating during day irradiation transients and extended it after sunset without decreasing thermal efficiency. Alqaed [95] investigated the effect of using a polymeric PCM in a solar hot air collector mounted on an inclined roof using the climatic conditions of Riyadh, Saudi Arabia. The

use of PCM causes the outlet air temperature to reduce in the early hours of the day, but the outlet temperature is enhanced in the last hours of the day. Wu et al. [96] studied the effect of thermophysical properties and melting temperature of PCM on the energy efficiency of ETSCs. The results indicated that the maximum outlet temperature of HTF and heat collection decreased by increasing several thermophysical properties and the melting temperature of PCM. Sadeghi et al. [97] added PCM to a direct ETC. The PCM (salt hydrate) was synthesized at various concentrations. It was observed that the thermal efficiency in the stagnation mode was improved from 66% to 82%.

Yeh et al. [98] tested a compact storage-integrated solar thermal collector design. The sodium acetate trihydrate (SAT) created a shape-stabilized PCM (ssPCMs). A numerical model has been used to study the PCM's (dis)charging behavior in a storage-integrated solar thermal collector composed of an evacuated tube and a double spiral coil heat exchanger. A geometrical optimization has been performed to achieve a 2.6 times longer discharging period with a minimum outlet temperature of 55 °C. Bejan et al. [99] conducted an experimental study of a transpired solar air collector with integrated PCM. The data show that, by implementing RT35 organic PCM (paraffin) within a real-scale solar collector, the maximum increase in temperature will be higher by 8.8%. In comparison, its performance coefficient will be 10.6% higher. Bouadila et al. [100] presented various designs of an ETSC thermally enhanced by adding reflectors and thermal storage units with NPCMs. The ETSC with a reflector was the most efficient compared to other systems and had the best energy-saving rates. Dinesh et al. [101] conducted an experimental study of the performance of a baffled solar-based air heater (SAH-BP) with organic phase-changing material (OPCM) back-up. The results showed that the use of OPCM within the baffled SAH enhanced its performance in terms of energy efficiency. The OPCM improved the energy efficiency of the SAH-BP by 11.25%. Nekoonam and Ghasempour [102] presented a 2-D concentric dispersion model with an apparent heat capacity method to investigate the thermal reactions of a solar system with thermal energy storage. The system consists of PCM or sensible, encapsulated spherical capsules and a synthetic oil operated as the HTF. The results showed that there was a 5% increase (decrease) in the input HTF temperature, the charging time was lowered (increased) by 25% (32%), and the total stored energy was increased by 20% (decreased by 17%).

Olfian et al. [103] evaluated a U-type of ETSC with a PCM. It was found that a 6 mm diameter yields a 13.5% improvement in the fluid outlet temperature in the charging process. It increased by 24% in the discharging process. Li et al. [104] developed a numerical study to determinate the thermal performance of a PCM-filled U-type ETSC with fins. It was found that the thermal efficiency of the ETSC was 50.72%. Sadeghi et al. [105] analyzed the recent investigations of single-unit PCM-based SC. Several SCs were reviewed. It was concluded that Paraffin wax was the highest PCM candidate used. Sethi et al. [106] reviewed recent studies incorporating PCM in ETSCs using air/water as a fluid and proposed the configuration for optimum performance. The outlet temperatures were significantly enhanced by maximizing the contact surface area between the PCM and the absorber plate. He et al. [107] analyzed an interlayer ventilated PCM component (IVPC) coupled with a solar air collector. It was found that IVPC may use solar energy to peak load shifting, reduce room temperature fluctuations, improve indoor thermal comfort, and provide solutions for farmhouses in cold regions to use clean energy for heating. Abu-Hamdeh et al. [108] studied a flat-plate solar panel collector with a PCM at the bottom. Three tubes were placed inside the PCM, on each of which fins were installed. It was found that using a larger diameter tube can cool the collector but make the outlet water temperature slightly lower. Hatamleh et al. [109] investigated the thermal behavior of glass in the presence of PCM (Decane) by molecular dynamics simulation. The atomic behavior of the structure is investigated by temperature and density profiles. It was concluded that using phase-change materials can prevent energy loss, reduce energy costs, and positively affect the appearance of the building.

5. Integration of PCMs in PV, CPV, and Hybrid PV/T Systems

Due to the competitive cost of producing electrical energy, PV systems are the fastest-growing solar technology worldwide. However, these systems are also applying PCMs to improve their performance. Figure 11 presents the basic scheme of PCM integrated into a solar PV panel to increase its electrical efficiency. It is well known that the electrical efficiency of a PV panel drops with its temperature increase. Therefore, a PCM is used to contain the temperature increase produced by the incoming solar radiation that cannot be converted into electricity by absorbing the thermal energy of the PV panel. The literature survey (Figure 12a) indicated that 45% of recent research is experimental, whereas 39% is theoretical–numerical, and 12% is a theoretical–experimental investigation. However, Figure 12b shows that 78% of researchers used organic, while 15% used composites and 7% inorganic PCMs.

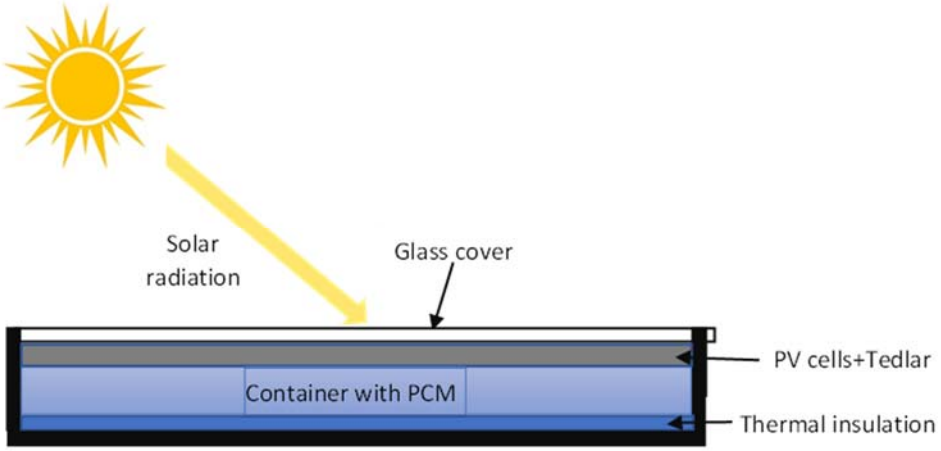

Figure 11. The basic scheme of a solar PV panel with PCM.

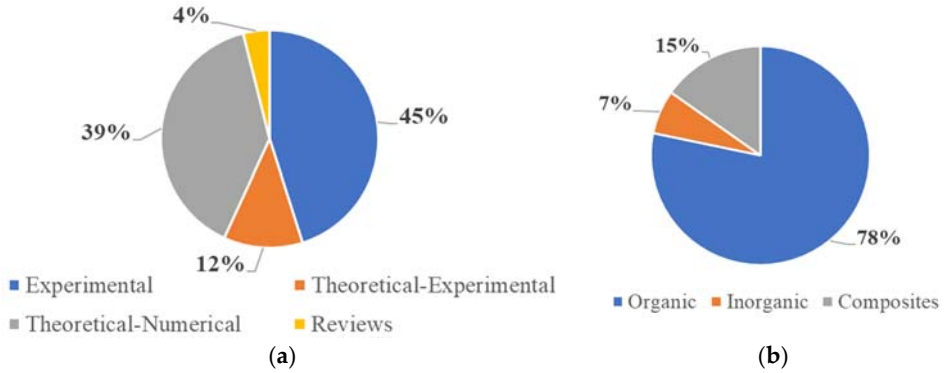

Figure 12. Classification of studies on integration of PCMs in PV, CPV, and hybrid PV/T systems. (**a**) Research approach and (**b**) PCM type.

Preet et al. [110] evaluated three different systems: (1) conventional PV panel, (2) water-based photovoltaic/thermal system (PV/T), and (3) water-based photovoltaic/thermal system with PCM. It was found that the maximum temperature reduction was 53% with the water-based PV/T-PCM. Al-Waeli et al. [111] analyzed a photovoltaic/thermal (PV/T) system. Three cooling systems were proposed: (1) a tank filled with water, (2) a tank filled with PCM, and (3) a tank filled with NPCM (SiC) and nanofluid (water-SiC). It was found that NPCM and nanofluid improved the electrical efficiency from 8.07% to 13.32%, compared with case 1. Nada et al. [112] studied the cooling and increase in efficiency of PV systems integrated into buildings by employing PCM and PCM with Al_2O_3 nanoparticles. The results showed that pure PCM and PCM with nanoparticles may reduce the module temperature between 8.1 and 10.6 °C and raise its efficiency by 5.7 and 13.2%, respectively. Khanna et al. [113] analyzed a PV–PCM system with fins to keep PV temperature low

during operation for different solar irradiance levels. The best spacing between fins was found to be 25 cm, whereas the best fin length was when it touched the bottom of the container. Darkwa et al. [114] investigated the integrated thermoelectric PCM system to enhance PV efficiency. The effect of various PCM thicknesses, conductivities, and phase change temperatures was evaluated. The simulation results showed the relevance of high PCM conductivity for a thick PCM layer to reduce its insulation effect on the thermoelectric generator (TEG) and PV layers.

Maatallah et al. [115] researched PVT–PCM/water systems. It was found that the addition of PCM enhanced thermal and overall efficiency by 26.87% and 40.59%, respectively, whereas the increase in electrical efficiency was 17.33%. Rajvikram et al. [116] presented a new method to increase the efficiency of a solar PV panel with PCM. The experiments were performed with two 5 W panels. The results indicated that PV–PCM with an aluminum sheet at the panel's backside enhances its efficiency by about 24.4%. Siahkamari et al. [117] experimentally investigated using a novel PCM in a PV module to control its temperature. Copper microchannel tubes with cold water flowing are in a box at the backside of the PV module. Pure sheep fat and sheep fat+CuO nanoparticles were contrasted with pure paraffin wax. It was found that experiments with sheep fat+CuO nanoparticles increased the peak power between 5.3% and 12%.

Soares et al. [118] reported an overview of the use of PCMs for the temperature control of PV systems. They described an experimental setup to compute the efficiency of commercial polycrystalline silicon PV panels with containers filled with PCM RT 22 HC on the backside of the panels. It was found that containers damage the performance of the PV/PCM systems. Akshayveer et al. [119] evaluated encapsulated PCM to enhance the efficiency of PV modules. It was found that in the new configuration, the temperature of PV cell temperature was reduced by 11.5%. Savvakis et al. [120] investigated the inclusion of PCMs through a tubular enclosure. Paraffins RT 27 and RT were used. It was observed that PV + PCM27 and PV + PCM31 systems enhanced energy generation by 4.19% and 4.24%, respectively. Elsheniti et al. [121] presented a one-dimensional mathematical model to forecast the module temperature (T_{pv}) with similar accuracy to CFD modeling but with a significant reduction in computational time. Abdollahi and Rahimi [122] studied a passive cooling system for PV modules. A novel geometry of the PCM enclosure was developed to enhance the heat transfer surface. The results showed that nano-composed PCM is more efficient than the plain one.

Mahdi et al. [123] employed several PCMs for cooling PV systems. The numerical simulations showed that the arrangement may extend the cooling duration, depending on the PV position and the number of PCMs. Akshayveer et al. [124] built and validated a computational model for a PV-T/PCM system. The PV/PCM system could reduce module temperature by 25% and 35%, concerning the PV system without PCM, and air PV-T/PCM, respectively. Consequently, the electrical efficiency of PV modules increased by 14.12% and 19.75% for PV/PCM systems and air PV-T/PCM, respectively. Xu et al. [125] experimentally evaluated the efficiency of a PV/T system coupled with an SC and with PCM. The results indicated that the temperature stratification of PCM was still significant in the solar collector even when metal fins were employed. It was found that the metal fins embedded in the PCM may not avoid its temperature stratification. Kumar et al. [126] conducted an experimental analysis with two prototypes. One consisted of a frame, a photovoltaic panel, and an electrical circuit with a specified charge, whereas the other was built with an aluminum container connected to the rear of the PV plate, which contains PCM. It has been shown that the efficiency of PV panels improved by an average of 4.3 percent when used with PCM. Carmona et al. [127] evaluated a new PCM and recovery system to enhance the overall efficiency of the SC. It was found that the daily electrical efficiency of the PVT–PCM system was enhanced by 7.43% concerning the typical PV module.

Abdulmunem et al. [128] analyzed the effect of tilt angle on the melting process of PCM used to cool a PV cell. It was observed that the increase in tilt angle reduces the melting time of PCM, provoking a diminution in the temperature of the PV module. Sudhakar et al. [129]

evaluated the use of PCM and natural water cooling to reduce the temperature of PV panels. They added OM 35 PCM at the tedlar surface, combined with water flow in the bottom of the PCM enclosure. It was concluded that the efficiency of the PV panel was enhanced by using the proposed cooling system. Rahmanian et al. [130] analyzed different passive cooling setups of a PV panel coupled with a solar concentrator (CPV). It was observed that the foam–PCM could reduce the average PV temperature by 10.7% compared with pure PCM. Savvakis and Tsoutsos [131] studied a PV/PCM system. The results showed that the operating temperature difference may increase to 26.6 °C, so the yearly power generation of the system increases by 5.7%. Duan [132] investigated, numerically and experimentally, the charging processes of PCM-porous systems with different inclined angles. The results showed that the inclined angle has little impact on the PCM-porous system with minor porosity, which is much different from the PCM-porous system with more significant porosity. Akshayveer et al. [133] developed a bifacial PV/PCM (BIF-PV/PCM) system. The enclosure's optimized bifurcated non-rectangular design was made to enhance incident radiation utilization. It was found that overall efficiency reached about 74%

Li et al. [90] analyzed a PVT system with PCM (PVT–PCM). The results of the cross-season test showed that the system's overall efficiency is 39.4%, and the energy-saving efficiency is 64.2%. Özbaş [134] made an experimental investigation of a thermosyphon (Ts) heat pipe for cooling a PV system. The results were compared with the use of a PCM. The best efficiency enhancement was obtained with the thermosyphon. Soliman et al. [135] reported a novel PV–PCM system design. It had an aluminum plate with holes and PCM. The arrangement with eight dimples provides a long thermal management duration and high electrical efficiency for the PV cell. Díaz et al. [136] evaluated several PV–PCM cooling systems. The results indicated that using PCM produced a maximum reduction in the PV module temperature of about 17.5 °C. Cui et al. [137] investigated the tube configuration, thermal fluid, and PCMs of a PV/T system. It was concluded that the PCM raised the electrical and thermal efficiency of the PV/T system by about 3–5% and 20–30%, respectively. Gad et al. [138] made an energy, exergy, and economic analysis of cooling PV panels with flat heat pipes (HPs) and PCM. The results showed that, compared with typical PV, the best PCM reached a maximum PV temperature reduction of 20.6 °C.

Kouravand et al. [139] evaluated five different PV cooling methods. The results showed that the concentrating PV-T (CPV-T) with nanofluid circulation and finned-PCM (CPV-T/NF/FPCM) produced the best cooling performance. Jahromi et al. [140] analyzed four nanomaterials to make NPCMs. The experimental results indicated that a mixture of GNP-CuO_3 produced a diminution of 6.6 °C in the PV module temperature. Nasef et al. [141] investigated a TES with PCM for cooling a PV system. The TES was fabricated of an acrylic heat exchanger (HE) with encapsulated PCM. The results showed that the best performance was obtained with the staggered alignment. Bhakre et al. [142] tested a PCM (Polyethylene Glycol 1500) with a metal matrix (MM) for cooling a PV system. The results indicated that using the PCM–MM decreased the PV panel temperature by 14.08% and increased the electrical efficiency by 8.87%. Kong et al. [143] studied a concentrating PV/T system with PCM (PV/T-CPCM). The maximum overall energy efficiency of the PV/T-CPCM system is about 7.9% and 10.7% higher than those of PV-CPC and PT-CPC systems, respectively. Colarossi et al. [144] built and tested a PV-PCM device for a year. The results showed that the proposed system reduces the impact of climate change by around 11.

Al-Najjar and Mahdi [145] developed an alternative mathematical model for PV/PCM. It was found that the model is reasonably accurate. However, the total simulation time was 2.2 h with a time step of 2.5 min, compared to 16 h for CFD. Azimi et al. [146] analyzed the effect of PCMs combined with a high thermal conductivity material to enhance their cooling capacity in PV modules. Composites of beeswax and coconut oil (BWCO) and their mixture with paraffin (PBWCO) acted as PCMs. Due to its high thermal conductivity, terephthalic acid powder (TPA) was added to PBWCO. It was concluded that adding TPA to PBWCO considerably increases its cooling capacity. Zohra et al. [147] proposed a system

combining two PCMs to enhance thermal performance in cooling PV modules. It was found that the electrical efficiency increased by 42.5% with two PCMs compared to PV without PCM. Wen et al. [148] presented an analysis of a novel concentrated system that consists of a photovoltaic/thermal (PV/T) module with PCM and an STC with thermoelectric generators (TEGs) connected in series. It was concluded that increasing the PCM thickness leads to a slight drop in the thermal efficiency, and even the electrical efficiency increases as the thickness increases. The overall efficiency shows a decreasing trend. Xiao et al. [149] reviewed recent studies in PV/T-PCM systems. The investigations on the cooling performance of the PCM in various PV/T collectors were analyzed. Challenges and suggestions were provided for developing PV/T-PCM systems. Luo et al. [150] developed a numerical model to investigate a PV–PCM system coupled with a thermoelectric (TE) module. The results showed that the solar cell temperature of the PV-PCM-TE system decreased by about 22 °C, in contrast with a PV system.

He et al. [151] made a two-dimensional model for a PV–PCM–TE system. The results showed that PCM could significantly enhance the total efficiency but cause power density to dramatically decrease. However, the optimum geometric parameters were derived from achieving the best power generation efficiency and density. Amalu and Fabunmi [152] investigated the use of Docosane $C_{22}H_{46}$ paraffin wax PCM to reduce the temperature of c-Si PV modules. The use of PCM increased the PV module efficiency by about 10.88%. In addition, it was found that the PV–PCM module is 1.05% more efficient and has a 34.0% longer fatigue life. Gao et al. [153] developed a detailed 3D transient model of PCM in a PV–TEG system. The influence of the PCM height and insertion position of the PCM in the PV–TEG system was analyzed. It was concluded that the PVPCM–TEG system had a higher overall performance than the PV–TEG–PCM system. Colarossi and Principi [154] experimentally investigated the yearly performance of a PV–PCM system coupled to a water tank to provide thermal energy for the domestic hot water (DHW) service of a typical residential building. It was observed that the PV–PCM and water tank system reached the maximum efficiency of 38% under summer climatic conditions. Li et al. [155] evaluated a coupled system consisting of PV direct driven air conditioners (PVACs), PCMs, and load flexibility for an office building. According to the influence on the zero energy probability (ZEP), the key parameters of the coupling system were ranked as follows: PVF > PCM melting temperature > PCM thickness.

Homlakorn et al. [156] evaluated a finned container filled with PCM located on the back surface of a PV module for cooling. The PCM is a mixture of myristic acid and stearic acid. It was found that the 60:40 wt% mixture produces the best results, with a reduction of 7.06 °C in the PV module temperature and an increase of 4.2% in its efficiency. Bria et al. [157] investigated a system with an aluminum plate attached to fins and a layer of PCM located on the backside of a PV panel. It was found that combining PCM and fins reduced the PV cell's temperature by 32 K compared to the typical module. Foteinis et al. [158] examined the performance of PV panels cooled with PCMs. It was found that cooling increases the panel's energy output by about 9.4%. However, payback time increased by almost nine years compared to the typical PV system. Lv et al. [159] developed a three-dimensional model for a PV–TEG–PCM system. The results showed that the performance of the PV–TEG–PCM system is better than that of PV–TEG or PV systems. Zhang et al. [160] developed a PV–PCM system with copper fins. It was found that the fin number played a more significant role in the cooling of the PV module.

6. Integration of PCMs in Solar Desalination Systems

The following are some recent studies focused on solar stills assisted with PCM (SSPCM) that operate in passive and active mode (Figure 13), emphasizing the improvement of the overall freshwater productivity (FWAP), efficiencies, and costs of freshwater production per liter (CPL). In Figure 13a, the diagram of single-slope passive solar still is presented, in which PCM has been integrated into the bottom of the saltwater storage tank. The solar energy captured by the saltwater and the PCM increases the system's

temperature, accelerating the evaporation rate. The water vapor flows throughout the interior space of the solar still, and a portion of it comes into contact with the glass cover (1). The vapor mass that reaches the inner surface of the glass cover releases thermal energy into the environment, resulting in the condensation of fresh water. Due to gravity and the slope of the glass cover, freshwater flows down to a set of containers outside the solar still (2)–(4). In Figure 13b, a schematic of an active solar still (single-slope) coupled with other technologies such as photovoltaic (PV) panels, flat plate solar collectors (FPSCs), and heat exchangers is presented. The main task of the FPSC is to increase solar energy capture outside the still and then supply it to the SSPCM through a working fluid (HTF). The objective of the PV module is to provide electrical energy to pump saline water. Finally, the main task of the PCM is to store thermal energy during the day from the sun and then use it during the night to increase the FWAP efficiencies and reduce the CPL.

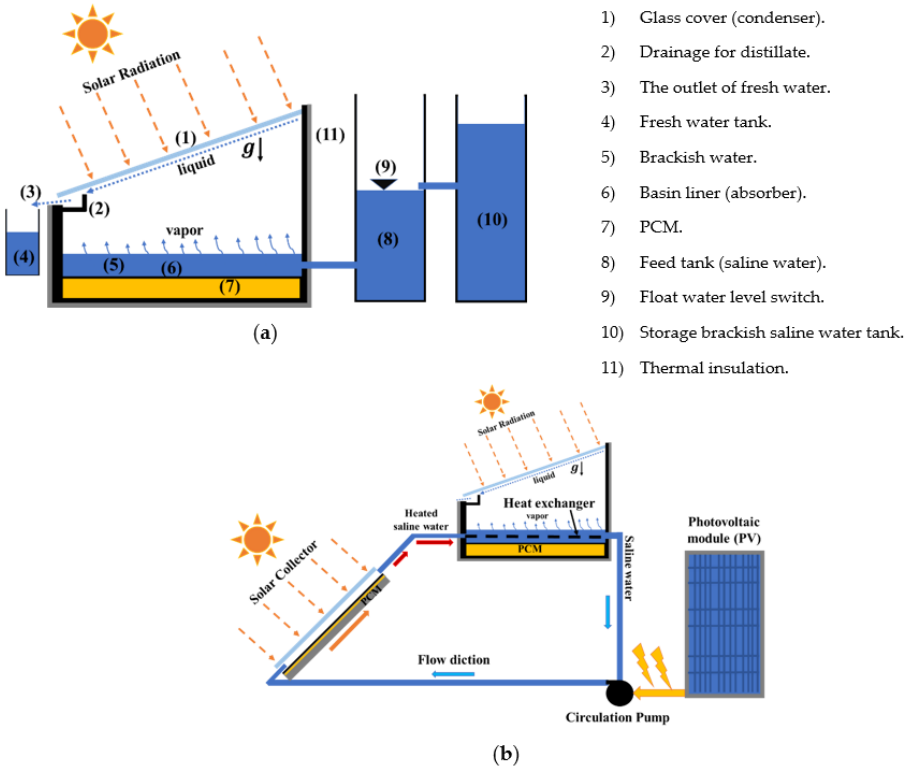

Figure 13. Schematic systems of desalination systems with PCMs: (**a**) passive system (single-slope solar still), (**b**) active system (single-slope solar still coupled to solar collector).

Sarhaddi et al. [161] compared the productivity of CaSS without and with PCMs under different weather conditions (sunny and semi-cloudy days). They found that the cumulative freshwater productivity (FWAP) with PCM on the semi-cloudy days was 4.94 kg/m^2·day, and without PCM it was 3.84 kg/m^2·day. Arunkumar and Kabeel [162] studied the PCM effect of a CTSS coupled with a CPC. The results showed FWAP values of 5.78 and 5.33 L/m^2·day, with the proposed system with PCM and without PCM, respectively. Faegh and Shafii [163] investigated the performance of a novel PCM-assisted solar still (SSPCM). The proposed technology does not affect performance during the day. The proposed SSPCM caused an 86% increase in achievement concerning the system without PCM, in which the FWAP value was 6.56 kg/m^2·day with an efficiency of 50%. Kabeel and Abdelgaied [164] coupled a parabolic trough (PTC) to an SSPCM. They found that the FWAP value was 10.77 L/m^2·day and 4.48 L/m^2·day, with 25.73% and 46% efficiencies for the SSPCM + PTC and CSS, respectively. Kabeel et al. [165] evaluated the efficiency and production of an SSPCM coupled with a parabolic dish solar collector (PDC). The FWAP value was 7 L/m^2·day for the proposed system and 4.25 L/m^2·day for the conventional system.

Sharshir et al. [166] implemented graphite nanoparticles (FGNs) and a film cooling system on the SSPCM. They observed that the proposed system increased the FWAP by 73.8% compared to the conventional SS, which presented a value of 2.116 L/m^2·day. Alharahsheh et al. [167] coupled a solar collector (SC) and a film cooling system on the SSPCM. They observed that the FWAP value was proportional to the ambient temperature and cooling volumetric flow. The proposed system presented an FWAP value of 4.3 L/m^2·day, of which 40% was obtained by thermal storage. Mazraeh et al. [168] integrated different types of semitransparent photovoltaic cells (condenser) and evacuated tubes (solar collector) on an SSPCM. The researchers observed that incorporating PCM increments the energy efficiency but not the exergetic efficiency, that the type of PV module does not affect the FWAP, but the electrical energy produced does, and that the greater the number of evacuated tubes, the greater the FWAP, but the less energy and exergetic efficiency. They found that the best-studied configuration developed an FWAP value of 4.55 kg/m^2·day, equivalent to 20.32% higher than the case without PCM. Abu-Arabi et al. [169] carried out a numerical study of an SSPCM assisted by a solar collector. They observed that adding a large mass of PCM to the system causes FWAP reductions. On the other hand, they observed an increase in the FWAP by increasing the cooling water flow. Dsilva Winfred Rufuss et al. [170] fabricated three types of NPCMs, embedded TiO_2, CuO, and GO nanoparticles in paraffin, and studied their effects on the performance of SSNPCMs. They reported FWAP values of 3.92, 4.94, 5.28, and 3.66 L/m^2·day for the NPCM, TiO_2, CuO, and GO systems, respectively. Elbar and Hassan [171] used the electricity generated by a PV system to provide additional heat to the saline water. They implemented a forced air-cooling system on condenser glass (FAC). They found that adding PCM in these technologies (SS, SS + PV, SS + PV + FAC) increases the value of the FWAP by 9, 11.7, and 5.9%, respectively. The highest FWAP (3 L/m^2·day) was achieved with the SS + PV + FAC + PCM system.

Safaei et al. [172] enhanced the efficiency and productivity of SSPCMs through the use of nanoparticles of graphene oxide (GO/Paraffin). They observed that the NPCM improved the FWAP by 25% concerning the system with pure PCM. Kumbhar [173] investigated the performance of reflectors on double-slope SSPCM over two high TDS water samples, one at 780 and the other at 820 TDS. The study showed that the developed technology improved the thermal efficiency of the conventional system by 1.4% and 0.79% for concentrations of 780 and 820 TDS, respectively. Vigneswaran et al. [174] compared three methods, without PCM, with only PCM, and with a combination of two PCMs, and their developed FWAP values were 3.68, 4.02, and 4.4 L/m^2·day, respectively. The exergetic efficiencies were 3.92% (without PCM), 3.23% (one PCM), and 3.52% (mixed PCMs). The researchers demonstrated that an appropriate combination of different PCMs is favorable for increasing the FWAP. Cheng et al. [175] developed a new PCM with a thermal conductivity of 1.5 W/m·K and a solar absorption of 0.94. The PCM is a composite material of paraffin wax, HDPE, and expanded graphite. The researchers replaced the conventional SS absorber plate with the new PCM. The experimental results presented an FWAP value of 3.41 L/m^2·day, representing an increase of 43.3% concerning the SS without PCM. Mousa et al. [176] filled black copper tubes with PCM and immersed them in saline water. The researchers tested different ratios between PCM and saline water masses (R). They found that the FWAP was inversely and directly proportional to the R value during the day and night. They published FWAP values of 2.15 and 1.86 L/m^2·day for R ratios of 0.17 and 0.35, respectively.

Yousef et al. [177] implemented hollow cylindrical pin fins embedded in PCM. They compared three systems: conventional SS, SSPCM, and finned SSPCM. They observed that the finned system presented an FWAP of 3.81 kg/m^2·day, higher than the FWAP of the conventional SS and the SSPCM by 17% and 7%, respectively. Khairat Dawood et al. [178] proposed an assisted SSPCM with PCM-filled ETSC with copper tube (U type), PTC, and heat exchange serpentine. They tested the effect on the FWAP when operating the proposed system with different HTFs such as water, oil, and nano-oil (CuO nanoparticles). They found that the proposed method (nano-oil) and the CSS developed FWAP values of 11.14

and 3.182 L/m^2·day, respectively. They also obtained the costs per liter (CPL) of fresh water for the conventional system and the one proposed (nano-oil) with values of 0.02 and 0.0154 USD/L, respectively. Kabeel et al. [179] compared three tubular solar stills, conventional system (TSS), TSSPCM, and TSSNPCM (with graphene oxide nanoparticles). The researchers observed that when the PCM had a higher thermal conductivity, the mass of steam generated was also higher. The FWAP values obtained were 2.59, 3.35, and 5.62 kg/m^2·day with thermal efficiencies of 23.48, 30.31, and 50.85% for the TSS, TSSPCM, and TSSNPCM, respectively. Kabeel et al. [180] found that the proposed system (TSS with PCM-filled copper tubes) presented an FWAP value of 9.05 L/m^2·day with an efficiency of 72.7%. In comparison, the conventional system gave an FWAP value of 4.31 L/m^2·day with an efficiency of 33.8%. The researchers concluded that PCM-filled copper tubes are an alternative to improve the performance of TSS.

Thalib et al. [181] evaluated tubular solar still assisted with NPCM (GO nanoparticles). They found that the proposed system developed an FWAP value of 20 L/m^2·day with an efficiency of 59%. Kabeel et al. [182] compared the performance of three solar pyramid stills (PSSs), conventional PSSs, hollow circular finned PSSs (FPSSs), and hollow circular fins whit PCM (FPSSPCM). They detected that the FPSSPCM system generated the highest FWAP with 8.1 L/m^2·day, followed by the FPSS with 5.75 L/m^2·day and finally, the CPSS with 4.02 L/m^2·day. They also estimated the CPL for the CPSS, FPSS, and FPSSPCM, obtaining CPL values of USD 0.0227, 0.025, and 0.019, respectively. Abu-Arabi et al. [79] proposed an assisted SSPCM with air glass cooling, solar collector, and PV modules. They also tested three PCMs (sodium acetate trihydrate, sodium thiosulfate pentahydrate, and paraffin wax). The proposed system reached an FWAP value of 6.3 L/m^2·day, while the simple system obtained an FWAP of 2.8 L/m^2·day. Furthermore, they concluded that the best PCM was the one with the highest temperature and latent heat of fusion. Ghadamgahi et al. [183] studied multistage solar still coupled to a solar collector with PCM. They observed that the FWAP increased by 15% with a thickness of 2.5 cm of PCM concerning the system without PCM. They found that the maximum FWAP was 4.9 L/m^2·day, obtained with a flow rate of 1.3 L/min. Hedayati-Mehdiabadi et al. [184] investigated the exergetic performance of a double-slope SS with PCM coupled to a PV/T collector during winter and summer. They observed that by increasing the mass flow in the PV/T collector, the FWAP and the exergetic efficiency increased in the SSPCM. They reported that the highest FWAP value developed during summer with 6.5 kg/m^2·day, while for winter, it was 1.3 kg/m^2·day. They also found that the exergetic efficiency is lower in winter than in summer.

Hafs et al. [185] carried out a numerical study to evaluate the productivity of an SS coupled to a PTC through a heat exchanger. They tested different absorbers: flat, rectangular, triangular, and spherical. The proposed system with rectangular absorbent surfaces developed an FWAP of 15.39 kg/m^2·day compared to the conventional system with 2.37 kg/m^2·day. The researchers conclude that a passive SS with a rectangular surface receptor is the most appropriate for domestic use, while coupling a PTC with a rectangular absorber has the potential to be implemented in industrial applications. Abdullah et al. [186] used NPCM (CuO nanoparticles) and electric heaters powered by a photovoltaic module. They tested three different solar still systems, namely flat tray, corrugated tray, and conventional. The researchers reported that the best system was the corrugated tray with NPCM and electric heater. The FWAP and CPL values were 6.2 L/m^2·day and USD 0.025, respectively. On the other hand, the FWAP of the CSS and CTSS systems were 2.2 and 4.1 L/m^2·day, with CPL values of USD 0.028 and 0.022, respectively. Manoj Kumar et al. [187] tested three methods; CSS, PCMSS (paraffin), and NPCMSS (silica nanoparticles). It was found that the NPCMSS and the PCMSS improved the FWAP by 67.07% and 51.22% concerning the CSS (5.47 L/m^2·day), respectively. Abed et al. [188] proposed a modified solar still coupled with a high-frequency ultrasonic vaporizer, PCM capsules, a solar collector, and a photovoltaic panel. They observed that the PCM cylindrical capsules increased the FWAP by 30.6% while incorporating the solar water heater and that the high-frequency ultrasonic vaporizer generated an increase of 415% concerning

the CSS. The estimated CPL values were USD 0.037 and 0.028 for CSS and the proposed system, respectively.

Elashmawy et al. [189] coupled a PTC and a PCM tube set into a tubular solar still. The tubes are black-painted aluminum filled with PCM with copper rods immersed in the PCM. The proposed system presented a value of the FWAP, efficiency, and CPL of fresh water of 5.55 L/m^2·day, 44.1%, and USD 0.00782, respectively. In comparison, the TSS without PCM tubes obtained a value of the FWAP, efficiency, and CPL of fresh water of 3.95 L/m^2·day, 31.9%, and USD 0.0163. Khalilmoghadam et al. [190] proposed an improved SSPCM with pulsating heat pipes. The results showed an efficiency of 48.5% for the proposed design, while the conventional solar still presented an efficiency of 23.7%. The proposed method gave an FWAP of 6.3 kg/m^2·day, with a CPL value of USD 0.0093. Sonker et al. [191] performed experiments to compare the performances of CSS, SSPCM, and SSNPCM (CuO nanoparticles). They found that the daily productivity of SSPCM and SSNPCM increased by 40.5% and 94.19% compared to CSS. The FWAP was 1.98, 2.782, and 3.845 L/m^2·day for the CSS, SSPCM, and SSNPCM systems. Younes et al. [192] investigated the performance of four solar stills: flat wick solar still (FWSS), corrugated wick solar still (CWSS), a half barrel wick solar still (BWSS), and a conventional solar still (CSS). They added NPCM (CuO nanoparticles) in the CWSS and BWSS systems, and they observed that the FWAP increased by 134% and 124% concerning the CSS, respectively. The FWAP values for CSS and CWSSNPCM were 2.4 and 5.6 L/m^2·day, respectively. They also reported the efficiency and CPL of fresh water, of which the CSS and CWSSNPCM systems presented values of 35% with USD 0.028, and 54.5% with USD 0.023, respectively. Agrawal and Singh [193] evaluated the performance of a double-slope solar still enhanced with a binary eutectic PCM and steel wool fiber (SWF). The binary eutectic PCM was stored in copper tubes and cylinders. The SWF was placed on the PCM containers. The proposed system presented the best results when operating with a 2 cm depth of saline water, developing an FWAP value of 3.4 kg/m^2·day and average energy and exergy efficiencies of 41% and 11.8%, respectively.

Suraparaju and Natarajan [194] applied solid staggered fins inserted in the PCM bed in an SS (single-slope type). They observed that the best performance was presented with a 2 cm depth of saline water. The systems obtained FWAP values of 3.75 and 3.017 L/m^2·day for the SSPCM and CSS, respectively. They also determined that the CPL of fresh water produced was 0.028 USD/m^2 and 0.03 USD/m^2 from the SSPCM and CSS, respectively. Abed and Hachim [195] evaluated the performance of a TSS with a rectangular pond painted black under the influence of two PCMs (paraffin and stearic acid). They found a curve of the FWAP as a function of the PCM mass, where the maximum point was reached with a thickness of 40 mm for both PCMs. They found that the proposed system with paraffin wax and stearic acid developed an FWAP of 8.1 and 7.7 L/m^2·day, respectively. In contrast, the TSS without PCMS obtained an FWAP of 6.95 L/m^2·day. Abdelgaied et al. [196] investigated circular and rectangular hollow copper fins, which were placed on the absorber surface of the tubular solar still and PCM below the absorber surface. They found that the TSSPCM with hollow circular fins obtained an FWAP value of 7.89 L/m^2·day, representing an improvement of 90.1%, concerning the TSS, which developed an FWAP value of 4.15 L/m^2·day. Jahanpanah et al. [197] implemented a commercial PCM with a melting point of 28 °C. They found that the system without PCM developed an FWAP value of 2.39 kg/m^2·day, while the systems with 3 and 6 kg of PCM obtained FWAP values of 2.58 and 3.11 kg/m^2·day, respectively. They observed that adding 6 kg of PCM improved the efficiency to 36.42%, starting from 28.13% (without PCM). They concluded that low melting point PCMs could be used efficiently to improve the performance of solar distillation.

Shoeibi et al. [198] implemented nanomaterials in the PCM (CuO and Al_2O_3 nanoparticles) and the solar absorber system (CuO nano coating). They placed anthracite as a solar-absorbing medium. The NPCM was placed inside copper tubes immersed in anthracite. They found that the proposed system presented FWAP values of 1.38 L/m^2·day, while the conventional system presented an FWAP value of 0.887 L/m^2·day. Jassim Jaber et al. [199] coupled a PTC to a double-slope solar still through a water tube connected to a heat ex-

changer immersed in the PCM. They reported that, with a depth of 20 mm of saline water, the proposed and conventional systems achieved FWAP values of 4.97 and 3.62 L/m^2·day, respectively. Vigneswaran et al. [200] compared three experimental systems, a CSS made of galvanized iron, an SS with galvanized iron and PCM (GIBSS), and another made of acrylic and PCM (ABSS). They found that the acrylic helped reduce the PCM charge interval and delayed the PCM discharge time, improving the still's performance. They found that the ABSS system presented an FWAP of 4.36 L/m^2·day, 10.1% and 19.1% higher than GIBSS and CSS, respectively. Parsa et al. [201] compared two experimental systems equipped with PCM, silver nanoparticles in black paint, and a turbulator with battery storage powered by photovoltaic. The difference between the systems is that one uses thermoelectric modules for heating (TEHM) and the other for cooling (TECM). The results showed that the TEHM system presents 20% and 7% more energy and exergy efficiency than the TECM systems. The best system concerning FWAP was the TEHM with PCM and turbulator, producing a value of 10.5 L/m^2·day. While for the same system without PCM, the FWAP was 7.5 L/m^2·day. Finally, the CPL for the TEHM and TECM systems was evaluated at USD 0.0127 and USD 0.023, respectively.

Kumar and Prakash [202] compared a conventional system (CSS), the conventional system plus PCM (CSSPCM), and the CSSPCM coupled with a SAH (CSSPCM + SAH). They observed that the CSSPCM + SAH system was the one that presented the best performance and efficiency. The proposed system developed an FWAP of 2.5 L/m^2·day, giving an increase in efficiency of 4.21% and 65.58% concerning the CSSPCM and CSS cases, respectively. Ho et al. [203] evaluated the productivity of a double-slope SSPCM coupled with a Fresnel lens (concentration of sunlight). The results showed a maximum value of the FWAP of 3.4 L/m^2 day. Moreno et al. [204] observed the effect of thermal energy storage by adding different PCMs (RT54HC, RT62HC, RT70HC, and RT80HC). They found that the best PCM was the RT70HC, generating an FWAP value of 5.42 kg/m^2·day with an efficiency of 66.7%. On the other hand, the system without PCM presented an FWAP of 4.53 kg/m^2·day with an efficiency of 55.78%. Selimefendigil et al. [205] investigated three methods: CSS, SSPCM, and an SSPCM with natural dolomite powder. The FWAP values were 3.84, 4.23, and 4.52 L/m^2·day for the CSS, SSPCM, and SSPCM systems integrated with natural dolomite powder, respectively. Using natural dolomite powder increased the energy and exergetic efficiencies of the CSS from 15.91% to 18.28% and from 1.26% to 1.78%, respectively. Ajdari and Ameri [206] studied an inclined-stepped SSPCM with baffles and different CuO and GO nanofluids. They found that the FWAP values for the best case were 16.99 and 12.79 L/m^2·day with and without PCM, respectively. They concluded that the CuO/GO nanofluid with PCM is a good candidate for improving their solar still productivity.

Moreno et al. [207] investigated the effect of the concentrations of salts in saline water on the FWAP. They found that the SSPCM, with pure water and 35 g/kg of TDS, developed an FWAP of 5.43 and 4.52 kg/m^2·day, respectively. While the CSS was under the same conditions, the FWAP values were 4.54 and 4.14 kg/m^2·day, respectively. The FWAP decreases when the salt concentration increases, and the presence of the PCM counteracts the thermal problems generated by the high salt contractions. Maridurai et al. [208] combined an FPC with PCM to a dual slope solar still. The FWAP values were 2.679 and 2.574 L/m^2·day for the proposed and conventional systems, respectively. Samuel Hansen et al. [209] studied a two-stage desalination system coupled with an inclined SSPCM to a CSS. The inclined SSPCM presents flat, steeped, and black fin-shaped absorbers staggered. Waste hot water from the sloped SSPCM is fed to the CSS to increase the FWAP. The proposed system generated a maximum FWAP value of 5.62 L/day. Hafs et al. [210] evaluated the efficiency of SS with rectangular channels filled with PCM during different year seasons. They found that the optimal proposed system presented FWAP values of 1.43, 0.71, 0.61, and 2.13 kg/m^2·day for the autumn, winter, spring, and summer seasons, respectively.

In Figure 14, four graphs are shown in which the bibliographic review of SSPCM systems studies has been classified. Figure 14a shows the participation by type of PCM. The

most studied PCM is paraffin wax and paraffin wax enhanced with nanoparticles (NPCMs with wt% ≤0.6), with a participation of 63.08% and 21.54%, respectively. It was found that 9.23% of the reviewed studies used inorganic salts as PCM, while the rest used other organic (4.62%) and inorganic (1.54%) PCMs. These results highlight that perhaps the significant difference in the popularity of PCM use is the cost and access to the material. Figure 14b shows that single-slope SSPCM and tubular SSPCM are the most studied technologies in the last ten years, with a participation of 64.1% and 12.5%, respectively. Followed by double-slope and cascade-type, with participations of 10.9% and 7.8%, respectively. However, pyramidal SSPCM is the least studied system, with a participation of 4.7%. It can be concluded that the simpler the system, the greater the opportunity to study and improve it. Therefore, much work remains regarding the rest of the technologies. In Figure 14c, a classification of the reviewed studies based on the mode of operation of the SSPCM is presented, which can operate passively or actively. Passive process refers to the operation of the SSPCM without the need to add an external source of electrical energy that promotes improving its thermal performance. As can be seen, 71.9% of the studies were passive systems, mainly focused on testing different PCMs and strategies to enhance heat transfer, such as fins and internal attachments. On the other hand, 28.1% of the studies were actively operated (active systems). They presented the peculiarity of being coupled to other technologies, mainly solar collectors such as CPC, PTC, Fresnel lens, FPSC, ETSC, PV/T modules, parabolic dish solar collectors, and reflector mirrors. These results could be seen mainly due to the costs associated with the manufacture of the device and the technical complexity related to the incorporation of other technologies. Finally, in Figure 14d, the reviewed works were classified based on the type of study performed. It was found that 83.02% of the studies were experimental, while 9.43% were based on numerical simulations using commercial software such as COMSOL Multiphysics and ANSYS FLUENT. Theoretical studies using energy balances had the lowest participation, representing 7.55%. From this section, it can be highlighted that numerical modeling and energy balance-based studies are still underexplored. This may be due to the physical phenomena's complexity and environmental effects. Therefore, experimental studies of SSPCMs seem to be less complicated. Next, a brief presentation of each investigation is presented.

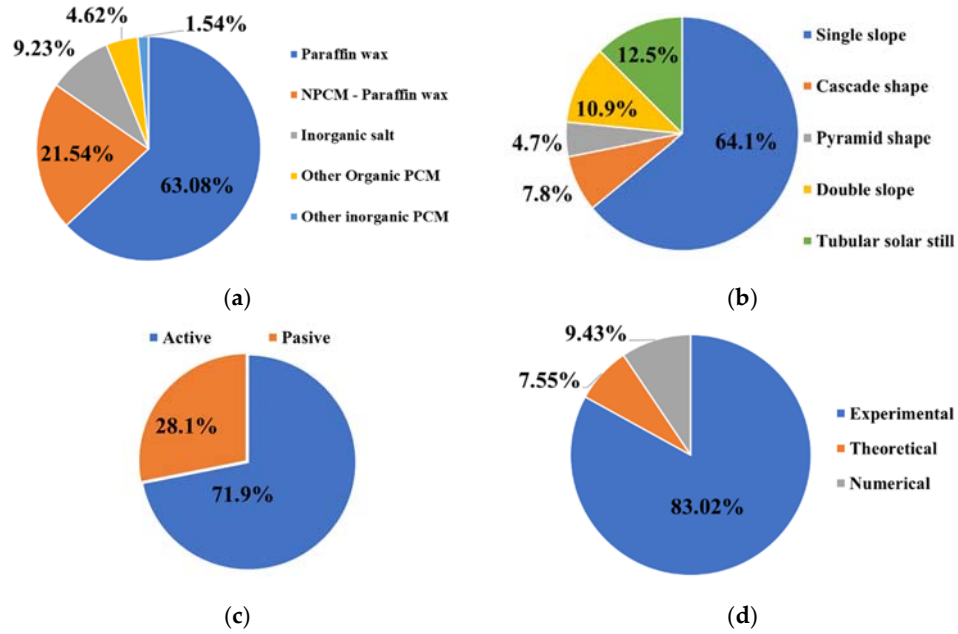

Figure 14. Classification of the bibliographic review of SSPCM studies: (**a**) by PCM type, (**b**) by technology type, (**c**) active and passive Systems, and (**d**) by study type.

7. Techniques for Improving Heat Transfer in PCMs Systems

From above, the most utilized PCMs for low-temperature applications are the organic solid–liquid ones. However, they have some disadvantages, too, such as low thermal conductivity [5]. Three primary techniques have been employed: fins within the PCM system, the NPCM system, and the metal foam PCM (MFPCM) system (Figure 15). These techniques are described in the following subsection.

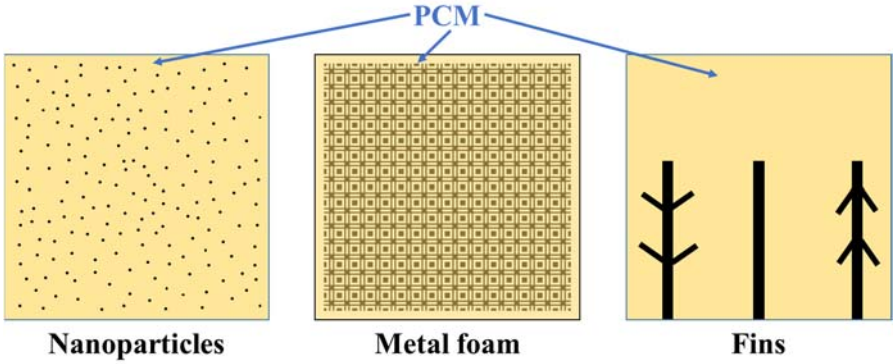

Figure 15. Example of enhancement added to PCM.

7.1. Finned PCM Systems

In heat transfer, fins are defined as surfaces extending from objects to increase the heat transfer rate. It happens with the increase in surface area. This subsection reviews recent studies exploring fins' use within latent heat storage units. An example of this usage is shown in Figure 15 (right).

Kuboth et al. [211] developed a simulation model to examine the effect of different fin distributions on the performance of shell-and-tube type latent thermal storage units at discharge. The heat exchanger pipe fin density was increased toward the pipe outlet. The concentration of fins was implemented linearly, exponentially, or suddenly. The PCM for this application had a melting temperature ranging from 40 to 44 °C. The average storage performance at total discharge only increased by three percent with the best allocation compared to an equidistant arrangement. Luo and Liao [212] introduced dendritic fins to improve the solid–liquid phase change in heat exchangers. The phase change temperature ranged from 42 to 44 °C. The results indicated that the dendritic fin enhanced the solid–liquid phase change in the heat exchanger for latent thermal storage. The presence of a dendritic fin led to the formation of multiple independent PCM zones. Zarei et al. [213] numerically studied the effects of copper fins' presence, configuration, and dimensions on a triplex tube containing PCM (melting temperature around 82 °C). Mixed fin configuration produced the highest storage when the fins were 28 and 1 mm long and wide, respectively. Liu et al. [214] investigated the performance of a PCM mesh-finned heat sink for the thermal management of thyristors. They experimented with PCMs with different melting temperatures from 43.5 to 150 °C. The PCM heat sink provided 80 s protection time and 100 s recovery time, demonstrating the excellent potential for this application.

Pakalka et al. [215] compared experimental and numerical natural convection heat transfer coefficients for the PCM melting process in a fin-and-tube copper heat exchanger. The PCM melting temperature ranged between 77 and 82 °C. The results were similar; the coefficients obtained experimentally and numerically were 61 and 68 W/m^2K, respectively. Ghalambaz et al. [216] developed and analyzed a three-dimensional model of a twisted-fin array for intensifying the charging response of PCM within a shell-and-tube storage system. They selected a PCM whose melting point is between 29 and 35 °C and compared the proposed configuration against straight fins and no-fins shell-and-tube storage systems. It was found that the energy charging time could be reduced by up to 42%, and the energy storage rate could be enhanced by up to 63%. Sun et al. [217] also analyzed a system with twisted fins but in a triple-tube latent heat energy storage. Torbarina et al. [218] developed a computational model to describe the heat transfer between HTF and PCM

in a tank (shell and tube) with straight fins. The PCM used had a melting temperature between 18 and 25 °C. Chen et al. [219] investigated the impact of bifurcated fins on melting and solidification processes and introduced an arc-shaped fin design to improve heat transfer. They utilized a PCM with a phase change temperature from 45 to 51 °C. The findings indicated that applying bifurcated fins could notably decrease the overall entropy generation. Furthermore, the energy storage time and the energy release time were reduced by 52.7 and 51.6%, respectively, with the implementation of concentric arc-shaped fins.

Privitera et al. [220] compared three axial heat conduction structures changed only for the fin shape (rectangular, trapezoidal, and fractal), using the commercial package ANSYS FLUENT for the use of energy storage systems. They used sodium nitrate ($NaNO_3$) as PCM. The fractal fin exhibited the highest discharging power (1136.6 W) against 950.8 and 979.4 W for rectangular and trapezoidal, respectively. Yu et al. [221] investigated the melting performance of a shell-and-tube thermal energy storage unit containing PCM with a rectangular fin configuration. The melting temperature of the PCM was between 48 and 50 °C. Their observations showed that the melting process was initially dominated by heat conduction and then by natural convection. They found that increasing the inlet temperature and reducing the flow rate of the HTF can enhance the energy efficiency of the PCM unit. Liu et al. [222] compared three PCM systems (no fins, circular fin, and spiral fin) for passive thermal management in cylindrical lithium–ion batteries. The utilized PCM had a melting point between 38 and 43 °C and a latent heat of 165 kJ/kg. The best performance was obtained with six turns of 6 mm width-spiral fins. Xu et al. [223] studied the melting rate of PCMs under different structural parameters (length, width, and position) of longitudinal rectangular fins in a horizontal shell-and-tube latent heat storage unit. The PCM used in their experiments had a melting temperature between 47.5 and 48.5 °C.

Rawat et al. [224] numerically analyzed the melting process of PCM in a rectangular enclosure using flanged fins to enhance melting. A double fin arrangement with upper and lower fins was employed, and various cases based on fin length ratio and material were examined with no-fin PCM enclosure. The result showed a high PCM melting rate for a low ratio and high thermal conductivity. Moreover, Cu fins outperformed other cases. The optimization concluded that a single flanged fin placed at the lower end of the container with a ratio of 0.55 has the minimum time (2338 s) and cost (0.229 USD/W). Firstly, Zhang et al. [213] compared and analyzed the thermal performances of nine new fins and the conventional straight fin. They secondly investigated the effects of transverse fin coverage area, number, arc length, thickness, and arc length of inner and outer arc fins on thermal performance, considering the impact of different heat transfer coefficients. The optimal fins kept the average cell temperature within 318.15 K, improved the heat transfer capability by 14.98%, extended the operating time by 131.5%, and reduced the system weight by 10.28%.

7.2. Nano-Enhanced PCM

Nanoparticles have a large surface-to-volume ratio. This high ratio makes them have specific properties. Nanoparticles can have a thermal conductivity of up to 5300 W/m.K depending on the material [225]. Adding nanoparticles to PCM produces a composite (NPCM) with affected thermophysical properties (Figure 15, left). The deposition of nanoparticles is crucial to fight against because if many nanoparticles stick together, the NPCM loses efficiency.

Prabakaran et al. [226] experimentally investigated the solidification behavior of functionalized graphene-based phase change nanocomposites inside a sphere (thermal transport and rheological characteristics). They obtained a maximum thermal conductivity enhancement of approximately 102 and 46%, with 0.5 vol% in the solid and liquid states, respectively. The rheological measurements showed that including nanoparticles led to the transition to non-Newtonian behavior. Pasupathi et al. [227] experimentally studied the influence of hybrid nanoparticles containing silicon dioxide (SiO_2) and cerium dioxide (CeO_2) nanoparticles on thermo-physical characteristics of the paraffin-based PCM.

They examined the synthesized samples under different instruments. The melting and solidification point was 63.74 °C. Mainly, the thermal conductivity of the paraffin was enriched up to 115.49% and 165.56%. Khan and Khan [228] integrated extended fins and graphene nanoparticles into the PCM to enhance thermal performance. The PCM used in their study had a melting temperature range from 41 to 44 °C, and they used different volume percentages of graphene nanoparticles (1, 3, and 5 vol%). The results showed that their proposed configuration could retrieve 11.15 MJ of thermal enthalpy in 1.08 h, significantly faster than the conventional shell-and-tube without fins. It takes 44.5 h to recover the same amount of thermal enthalpy. Mohaghegh et al. [229] studied the heat transfer of water jet impingement on a hot plate enhanced with a nano-encapsulated PCM slurry. The slurry contained polystyrene shells with n-octadecane paraffin wax as the core and aluminum oxide nanoparticles. They found that the maximum cooling performance was achieved with a 15% concentration of nano-encapsulated PCM. The study was focused on the laminar flow regime.

Zahid et al. [230] conducted an experimental study on the thermal behavior of a copper foam-based heat sink integrated with various concentrations (0.15, 0.20, and 0.25 wt%) of alumina nanoparticles and PCM (RT-54HC). The study showed a maximum reduction of 36.95% in the base temperature and a maximum improvement of 288% in the working time. The authors suggested the use of NPCMs in electronic cooling systems. John et al. [231] studied a battery thermal management system based on organic PCM (stearic acid) and copper oxide nanoparticles. They optimized the system for different PCM thicknesses of 2–12 mm and additive percentages of 0–6% of nanoparticles. The results showed that stearic acid-based PCM effectively controls cell temperature. The lowest cell temperature attained was found to be 311.93 K. Hayat et al. [232] incorporated multi-walled carbon nanotubes, graphene nano-platelets, and titanium oxide-based single and novel hybrid nano additives into paraffin to find the optimal composite which could not only enhance the thermal conductivity but also limit the latent heat. The results showed that the highest thermal conductivity value was observed at 1.0 wt% of graphene and multi-walled nanotube hybrid particles based PCM with a maximum enhancement of 170% at 25 °C. Moreover, titanium oxide nanoparticles showed the minimum reduction in the latent heat. They mentioned that nanofillers have the potential to be employed in thermal energy storage applications.

7.3. Metal Foam PCM

The enhancement of heat transfer by pouring PCM inside a metal foam structure is induced by conduction and convection. Metal foam assists the conduction mechanism, suppresses convective heat transfer, and its porous produces resistance to the free movement of liquid PCM. Higher porosity and lower pore density of MF can help mitigate the suppression of natural convection [233]. The way PCM fills the empty spaces inside metal foam is presented in Figure 15 (center).

Chen et al. [234] numerically investigated the energy transport inside a PCM-based thermal energy storage system using metal foam as an enhancement technique. The PCM changed its phase at 58 °C, approximately. The results showed that the overall performance improved by inserting metal foam in both HTF and PCM sides, and the time needed for the entire process decreased by 84.9% compared to the case of pure PCM. Mabrouk et al. [235] numerically investigated the two-dimensional laminar flow and the heat transfer in an open-ended rectangular porous channel (metal foam), including a PCM under forced convection. They found the foam pore effect on the phase change process under unsteady forced convection in a PCM-saturated porous channel. Ghalambaz et al. [236] studied the melting flow and heat transfer of copper-oxide coconut oil in thermal energy storage filled with a nonlinear copper metal foam. They investigated the effect of average porosity; porosity distribution; pore size density; the enclosure's inclination angle, and nanoparticles' concentration on the isotherms, melting maps, and melting rate. The coconut oil changed its phase at 24 °C. The results showed that the natural convection flows were weak in the metal foam and the variation in porosity from 0.825 to 0.9 changes the melting time by

about 116%. Ghalambaz et al. [237] investigated a thermal energy storage system consisting of a cylinder (filled with an inhomogeneous porous medium) with a longitudinal inner tube containing the HTF. They also used coconut oil loaded with copper nanoparticles. Their results showed that increasing nanoparticle volume fraction decreased the charging time.

Falcone et al. [238] showed the benefits that a 95% porous copper metal foam could bring to a PCM-based thermal storage system by simply loading it due to the increase in the effective thermal conductivity of the medium. They used a PCM in which phase change temperature ranged from 29 to 36 °C. They noticed that metal foam produced a more even temperature within the PCM. On the other hand, the melting time was reduced. Liu et al. [239] developed a heat storage system with metal foam and three structures (positive, negative, and no gradient) as an enhancer to save and deploy waste heat. The melting temperature of the PCM was between 46 and 55 °C. The total phase transition time was 12,470 s, 13,500 s, and 17,930 s in the cases of positive, no, and negative gradients, respectively. The initial investment increased by 76.09%, compared to not adding metal foam, but it was cost-effective in the long run of thermal cycles. Hassan et al. [240] used NPCM with copper foam to cool electronic devices. They combined PT-58 PCM with graphene nanoplatelets and magnesium oxide (MgO) nanoparticles. The research concluded that incorporating copper foam in the NPCM can effectively decrease the heat sink base temperature and provide the best cooling performance at low and high heating loads.

Chen et al. [241] experimentally and numerically studied the influence mechanism of the physical parameters of PCMs and structural parameters of metal foam on the melting of composite PCMs. The result showed that the porosity, the material of the metal foam, and the thickness of the metal foam were the main factors affecting the melting rate and heat transfer strength of PCMs. In contrast, the effect of pore density can be ignored. They analyzed and obtained three general correlations about the liquid fraction; Nusselt number with Fourier number, Stefan number, and Rayleigh number; and dimensionless structural parameters of metal foams. Sreenath and Chanda [242] studied the effect of ambient conditions and choice of PCM on the thermal performance of a metal foam composite heat sink. The PCMs considered were paraffin wax, docosane, and eicosane. The melting temperatures were 44.5–60.1 °C, 40.3–44.5 °C, and 36.3–38.1 °C, respectively. They found that the temperature uniformity within the heat sink cavity improved significantly in the presence of metal foam. However, due to the limit in thermal conductivity enhancement that can be achieved by introducing high thermally conductive foam material into the PCM material, similar behavior concerning the enhancement of temperature uniformity and attainment of maximum base temperature was observed with aluminum and copper foam PCM composite heat sinks.

8. Conclusions and Recommendations

From the overall reviewed studies, some conclusions and recommendations can be stated:

1. The addition of PCM in the building envelope can reduce the inner surface wall/roof temperature by up to 6.2 °C and increase the delay time by 0.5–4 h. The heat flux can be reduced by up to 97%. Therefore, the indoor temperature can be highly reduced, diminishing up to 56% of the energy consumption.
2. Solar collectors have enhanced their thermal efficiency and outlet temperature by about 11% using PCMs.
3. By using PCMs for cooling PV cells, considerable increases in electrical efficiency (some authors reported more than 30%) and decreases in module temperature (up to 20 °C) are accomplished.
4. Combined PV-Thermal systems (PVT) were beneficiated substantially with PCMs (some authors reported an increase in overall efficiency greater than 40%).
5. Adding any PCM in solar stills improves the production of total freshwater (FWAP), which on average was 3.82 L/m^{2}day and improved on average up to 4.95 L/m^{2}day.

The main task of the PCM was to store thermal energy during the day to use it later at night to increase FWAP.

6. The most used PCMs in analyzed low-temperature applications are Organics PCMS. In particular, the paraffin waxes. Even composites PCMs are mainly paraffin mixed with other particles. The most used materials to enhance paraffin were graphite, TiO_2, CuO, GO, Silica, and Al_2O_3.
7. PCM enhancements are adopted to increase thermal conductivity, and there are studies where it increased up to 1695%, but there is a consequence since it has been reported that the latent and specific heat suffer a decrease.
8. There are three methods widely used for modeling the heat transfer in PCMs: enthalpy, effective heat capacity, and the enthalpy–porosity method. The three have shown high accuracy when compared to experimental data. The enthalpy–porosity method includes a source term in momentum equations necessary when the buoyancy effect has to be considered.

In addition, there are recommendations for future work:

1. For building envelope applications, it is necessary to compare different ambient conditions because this parameter is predominant when selecting the right PCM.
2. Since using heat transfer enhancements in PCMs reduces heat loss in many applications, studying exergy-economic, enviro economic, and CO_2 mitigation parameters involving PCM and its enhancements are recommended, leading to environmentally effective designs.
3. The manufacture of NPCMs based on paraffin wax is a trend in analyzed solar technologies. Therefore, continuing to test other nanomaterials, nanocomposites, and nanofluids on this and other PCMs is an excellent opportunity to increase energy and exergetic efficiencies.
4. Few works have been given to improving the condenser element of solar stills, and PCMs have not been incorporated into cooling systems either, so involving other passive and/or active technologies assisted with PCMs is an option to improve their performance.
5. Most of the works reviewed are experimental, so it is advisable to continue developing theoretical and numerical methodologies that help predict various reliable scenarios of SSPCM systems to take the best ones through Pre-construction decisions and implementation.
6. For a future review analysis, comparing some of the widely used PCMs in terms of cost and performance is recommended.

Author Contributions: Conceptualization, J.F.H. and S.F.M.; writing—original draft preparation, J.F.H., S.F.M. and V.M.M.; writing—review and editing, J.F.H., S.F.M. and V.M.M.; supervision, J.F.H. All authors have read and agreed to the published version of the manuscript.

Funding: This research received no external funding.

Institutional Review Board Statement: Not applicable.

Informed Consent Statement: Not applicable.

Data Availability Statement: Not applicable.

Acknowledgments: The authors wish to acknowledge the support of the National Science and Technology Council of the Mexican Republic (CONACYT), given through its graduate grants program.

Conflicts of Interest: The authors declare no conflict of interest.

Abbreviations

BWCO	Beeswax and coconut oil
CaSS	Cascade solar stills
CFD	Computational fluid dynamics
CPC	Compound parabolic concentrating
CPV	Concentrator photovoltaic
CSS	Conventional solar still
CTSS	Concentric circular tubular solar still
EAHE	Earth to air heat exchanger
EG	Expanded graphite
ETC	Evacuated tube collector
ETC/S	Evacuated tube collector with storage
ETC/WS	Evacuated tube collector without storage
ETSC	Evacuated tube solar collector
FAC	Forced air-cooling
FGN	Flake graphite nanoparticles
FPC	Flat plate collector
FPCM	Finned phase change material
FPSC	Flat plate solar collector
FPSS	Hollow circular finned solar still
FPSSPCM	Hollow circular finned solar still with phase change material
FVM	Finite volume method
FWAP	Freshwater productivity
HDPE	High-density polyethylene
HE	Heat exchanger
HP	Heat pipe
HP/ETC	Heat pipe evacuated tube solar water heater collector
HTE	Heat transfer enhancements
HTF	Heat transfer fluid
IVPC	Interlayer ventilated phase change material component
MFPCM	Phase change material poured in metal foam
NF	Nanofluid
NPCM	Nano-enhanced phase change material
OPCM	Organic phase change material
PBWCO	Beeswax and coconut oil with paraffin
PCM	Phase change material
PSS	Pyramid solar stills
PTC	Parabolic trough collector
PV	Photovoltaic
PV/T	Photovoltaic and thermal
SAC	Solar air collector
SACSU	Solar air collector/storage unit
SAH	Solar air heater
SAH-BH	Baffled solar-based air heater
SC	Solar collector
SCC	Solar collector connected to an external collector
SS	Solar still
SSPCM	Solar still assisted whit phase change material
ST	Solar thermal
SWF	Steel wool fiber
TCE	Thermal conductivity enhancers
TEG	Thermoelectric generator
TES	Thermal energy storage
TSC	Transpired solar air collector
TSS	Tubular solar still

References

1. Ban, K.M. Sustainable Development Goals. *News Surv.* **2016**, *37*, 18–19.
2. Reddy, K.G.; Deepak, T.G.; Anjusree, G.S.; Thomas, S.; Vadukumpully, S.; Subramanian, K.R.V.; Nair, S.V.; Nair, A.S. On Global Energy Scenario, Dye-Sensitized Solar Cells and the Promise of Nanotechnology. *Phys. Chem. Chem. Phys.* **2014**, *16*, 6838–6858. [CrossRef]
3. Belyakov, N. Chapter Twenty-Three—Sustainable Electricity Management beyond Generation. In *Sustainable Power Generation*; Belyakov, N., Ed.; Academic Press: Cambridge, MA, USA, 2019; pp. 539–563, ISBN 978-0-12-817012-0.
4. Hussain, F.; Rahman, M.Z.; Sivasengaran, A.N.; Hasanuzzaman, M. Chapter 6—Energy Storage Technologies. In *Energy for Sustainable Development*; Hasanuzzaman, M.D., Rahim, N.A., Eds.; Academic Press: Cambridge, MA, USA, 2020; pp. 125–165, ISBN 978-0-12-814645-3.
5. Su, W.; Darkwa, J.; Kokogiannakis, G. Review of Solid-Liquid Phase Change Materials and Their Encapsulation Technologies. *Renew. Sustain. Energy Rev.* **2015**, *48*, 373–391. [CrossRef]
6. Javadi, F.S.; Metselaar, H.S.C.; Ganesan, P. Performance Improvement of Solar Thermal Systems Integrated with Phase Change Materials (PCM), a Review. *Sol. Energy* **2020**, *206*, 330–352. [CrossRef]
7. Laloui, L.; Rotta Loria, A.F. Chapter 1—Energy and Geotechnologies. In *Analysis and Design of Energy Geostructures*; Laloui, L., Rotta Loria, A.F., Eds.; Academic Press: Cambridge, MA, USA, 2020; pp. 3–23, ISBN 978-0-12-820623-2.
8. Altintas, H.I. Investigation of Zero Energy House Design: Principles Concepts Opportunities and Challenges. *Herit. Sustain. Dev.* **2019**, *1*, 21–32. [CrossRef]
9. Ermiş, K.; Findik, F. Thermal Energy Storage. *Sustain. Eng. Innov.* **2020**, *2*, 66–88. [CrossRef]
10. Guichard, S.; Miranville, F.; Bigot, D.; Malet-Damour, B.; Libelle, T.; Boyer, H. Empirical Validation of a Thermal Model of a Complex Roof Including Phase Change Materials. *Energies* **2016**, *9*, 9. [CrossRef]
11. Liu, P.-F.; Lin, Y.-P.; Tzeng, C.-T.; Lai, C.-M. Heat Transfer and Energy Performance of a PVA Wall Tile Containing Macro-Encapsulated PCM. *Energies* **2016**, *9*, 625. [CrossRef]
12. Chung, M.H.; Park, J.C. An Experimental Study on the Thermal Performance of Phase-Change Material and Wood-Plastic Composites for Building Roofs. *Energies* **2017**, *10*, 195. [CrossRef]
13. Mazzeo, D.; Oliveti, G.; Arcuri, N. A Method for Thermal Dimensioning and for Energy Behavior Evaluation of a Building Envelope PCM Layer by Using the Characteristic Days. *Energies* **2017**, *10*, 659. [CrossRef]
14. Reddy, K.S.; Mudgal, V.; Mallick, T.K. Thermal Performance Analysis of Multi-Phase Change Material Layer-Integrated Building Roofs for Energy Efficiency in Built-Environment. *Energies* **2017**, *10*, 1367. [CrossRef]
15. Zhou, Q.; Liu, P.-F.; Tzeng, C.-T.; Lai, C.-M. Thermal Performance of Microencapsulated Phase Change Material (MPCM) in Roof Modules during Daily Operation. *Energies* **2018**, *11*, 679. [CrossRef]
16. Bendic, V.; Dobrotă, D. Theoretical and Experimental Contributions on the Use of Smart Composite Materials in the Construction of Civil Buildings with Low Energy Consumption. *Energies* **2018**, *11*, 2310. [CrossRef]
17. Rashid, Y.; Alnaimat, F.; Mathew, B. Energy Performance Assessment of Waste Materials for Buildings in Extreme Cold and Hot Conditions. *Energies* **2018**, *11*, 3131. [CrossRef]
18. Ascione, F.; Bianco, N.; De Masi, R.F.; Mastellone, M.; Vanoli, G.P. Phase Change Materials for Reducing Cooling Energy Demand and Improving Indoor Comfort: A Step-by-Step Retrofit of a Mediterranean Educational Building. *Energies* **2019**, *12*, 3661. [CrossRef]
19. Moreno, S.; Hinojosa, J.F.; Hernández-López, I.; Xaman, J. Numerical and Experimental Study of Heat Transfer in a Cubic Cavity with a PCM in a Vertical Heated Wall. *Appl. Therm. Eng.* **2020**, *178*, 115647. [CrossRef]
20. Tsoka, S.; Theodosiou, T.; Papadopoulou, K.; Tsikaloudaki, K. Assessing the Energy Performance of Prefabricated Buildings Considering Different Wall Configurations and the Use of PCMs in Greece. *Energies* **2020**, *13*, 5026. [CrossRef]
21. Charvátová, H.; Procházka, A.; Zálešák, M. Computer Simulation of Passive Cooling of Wooden House Covered by Phase Change Material. *Energies* **2020**, *13*, 6065. [CrossRef]
22. Ho, C.-J.; Lin, S.-M.; Lai, C.-M. Effects of the Wall Properties on the Cooling Efficiency in a Thermosyphon Containing PCM Suspensions. *Energies* **2021**, *14*, 572. [CrossRef]
23. Rehman, A.U.; Ghafoor, N.; Sheikh, S.R.; Kausar, Z.; Rauf, F.; Sher, F.; Shah, M.F.; Yaqoob, H. A Study of Hot Climate Low-Cost Low-Energy Eco-Friendly Building Envelope with Embedded Phase Change Material. *Energies* **2021**, *14*, 3544. [CrossRef]
24. Ye, R.; Fang, X.; Zhang, Z. Numerical Study on Energy-Saving Performance of a New Type of Phase Change Material Room. *Energies* **2021**, *14*, 3874. [CrossRef]
25. Rehman, A.U.; Sheikh, S.R.; Kausar, Z.; McCormack, S.J. Numerical Simulation of a Novel Dual Layered Phase Change Material Brick Wall for Human Comfort in Hot and Cold Climatic Conditions. *Energies* **2021**, *14*, 4032. [CrossRef]
26. Kavgic, M.; Abdellatef, Y. Temperature Control to Improve Performance of Hempcrete-Phase Change Material Wall Assemblies in a Cold Climate. *Energies* **2021**, *14*, 5343. [CrossRef]
27. Kobeyev, S.; Tokbolat, S.; Durdyev, S. Design and Energy Performance Analysis of a Hotel Building in a Hot and Dry Climate: A Case Study. *Energies* **2021**, *14*, 5502. [CrossRef]
28. Zhou, H.; Fransson, Å.; Olofsson, T. An Explicit Finite Element Method for Thermal Simulations of Buildings with Phase Change Materials. *Energies* **2021**, *14*, 6194. [CrossRef]

29. Baccega, E.; Bottarelli, M. Granular PCM-Enhanced Plaster for Historical Buildings: Experimental Tests and Numerical Studies. *Energies* **2022**, *15*, 975. [CrossRef]
30. Cui, H.; Yu, S.; Cao, X.; Yang, H. Evaluation of Printability and Thermal Properties of 3D Printed Concrete Mixed with Phase Change Materials. *Energies* **2022**, *15*, 1978. [CrossRef]
31. Bruno, R.; Bevilacqua, P.; Rollo, A.; Barreca, F.; Arcuri, N. A Novel Bio-Architectural Temporary Housing Designed for the Mediterranean Area: Theoretical and Experimental Analysis. *Energies* **2022**, *15*, 3243. [CrossRef]
32. Liu, Z.-A.; Hou, J.; Chen, Y.; Liu, Z.; Zhang, T.; Zeng, Q.; Dewancker, B.J.; Meng, X.; Jiang, G. Effectiveness Assessment of Different Kinds/Configurations of Phase-Change Materials (PCM) for Improving the Thermal Performance of Lightweight Building Walls in Summer and Winter. *Renew. Energy* **2023**, *202*, 721–735. [CrossRef]
33. Hou, J.; Liu, Z.-A.; Zhang, L.; Zhang, T.; Hou, C.; Fukuda, H. Parametric and Economic Analysis of Incorporating Phase Change Material (PCM) into Exterior Walls to Reduce Energy Demand for Traditional Dwellings in Northeast of Sichuan Hills, China. *Appl. Therm. Eng.* **2023**, *223*, 119982. [CrossRef]
34. Terhan, M.; Ilgar, G. Investigation of Used PCM-Integrated into Building Exterior Walls for Energy Savings and Optimization of PCM Melting Temperatures. *Constr. Build. Mater.* **2023**, *369*, 130601. [CrossRef]
35. Xiong, Q.; Alshehri, H.M.; Monfaredi, R.; Tayebi, T.; Majdoub, F.; Hajjar, A.; Delpisheh, M.; Izadi, M. Application of Phase Change Material in Improving Trombe Wall Efficiency: An up-to-Date and Comprehensive Overview. *Energy Build.* **2022**, *258*, 111824. [CrossRef]
36. Liu, X.; Zhou, Y.; Li, C.-Q.; Lin, Y.; Yang, W.; Zhang, G. Optimization of a New Phase Change Material Integrated Photovoltaic/Thermal Panel with The Active Cooling Technique Using Taguchi Method. *Energies* **2019**, *12*, 1022. [CrossRef]
37. Tenpierik, M.; Wattez, Y.; Turrin, M.; Cosmatu, T.; Tsafou, S. Temperature Control in (Translucent) Phase Change Materials Applied in Facades: A Numerical Study. *Energies* **2019**, *12*, 3286. [CrossRef]
38. Szyszka, J.; Bevilacqua, P.; Bruno, R. An Innovative Trombe Wall for Winter Use: The Thermo-Diode Trombe Wall. *Energies* **2020**, *13*, 2188. [CrossRef]
39. Leang, E.; Tittelein, P.; Zalewski, L.; Lassue, S. Impact of a Composite Trombe Wall Incorporating Phase Change Materials on the Thermal Behavior of an Individual House with Low Energy Consumption. *Energies* **2020**, *13*, 4872. [CrossRef]
40. Lichołai, L.; Starakiewicz, A.; Krasoń, J.; Miąsik, P. The Influence of Glazing on the Functioning of a Trombe Wall Containing a Phase Change Material. *Energies* **2021**, *14*, 5243. [CrossRef]
41. Kong, X.; Li, J.; Fan, M.; Li, W.; Li, H. Study on the Thermal Performance of a New Double Layer PCM Trombe Wall with Multiple Phase Change Points. *Sol. Energy Mater. Sol. Cells* **2022**, *240*, 111685. [CrossRef]
42. Sheikholeslami, M.; Al-Hussein, H.R.A. Modification of Heat Storage System Involving Trombe Wall in Existence of Paraffin Enhanced with Nanoparticles. *J. Energy Storage* **2023**, *58*, 106419. [CrossRef]
43. Zhou, S.; Bai, F.; Razaqpur, G.; Wang, B. Effect of Key Parameters on the Transient Thermal Performance of a Building Envelope with Trombe Wall Containing Phase Change Material. *Energy Build.* **2023**, *284*, 112879. [CrossRef]
44. Omara, A.A.M.; Mohammed, H.A.; Al Rikabi, I.J.; Abuelnour, M.A.; Abuelnuor, A.A.A. Performance Improvement of Solar Chimneys Using Phase Change Materials: A Review. *Sol. Energy* **2021**, *228*, 68–88. [CrossRef]
45. Thantong, P.; Khedari, J.; Chantawong, P. Investigation of Thermal Performance by Applying a Solar Chimney with PCM towards the Natural Ventilation of Model House under Climate of Thailand. *Mater. Today Proc.* **2018**, *5*, 14862–14867. [CrossRef]
46. Xamán, J.; Vargas-López, R.; Gijón-Rivera, M.; Zavala-Guillén, I.; Jiménez, M.J.; Arce, J. Transient Thermal Analysis of a Solar Chimney for Buildings with Three Different Types of Absorbing Materials: Copper Plate/PCM/Concrete Wall. *Renew. Energy* **2019**, *136*, 139–158. [CrossRef]
47. Tiji, M.E.; Eisapour, M.; Yousefzadeh, R.; Azadian, M.; Talebizadehsardari, P. A Numerical Study of a PCM-Based Passive Solar Chimney with a Finned Absorber. *J. Build. Eng.* **2020**, *32*, 101516. [CrossRef]
48. Ashouri, M.; Hakkaki-Fard, A. Improving the Performance of the Finned Absorber Inclined Rooftop Solar Chimney Combined with Composite PCM and PV Module. *Sol. Energy* **2021**, *228*, 562–574. [CrossRef]
49. Li, W.; Li, Z.; Xie, L.; Li, Y.; Long, T.; Huang, S.; Lu, J.; Wang, Z. Evaluation of the Thermal Performance of an Inclined Solar Chimney Integrated with a Phase Change Material. *Energy Build.* **2022**, *270*, 112288. [CrossRef]
50. Nateghi, S.; Jahangir, M.H. Performance Evaluation of Solar Chimneys in Providing the Thermal Comfort Range of the Building Using Phase Change Materials. *Clean. Mater.* **2022**, *5*, 100120. [CrossRef]
51. Rodrigues, L.T.; Gillott, M. A Novel Low-Carbon Space Conditioning System Incorporating Phase-Change Materials and Earth–Air Heat Exchangers. *Int. J. Low-Carbon Technol.* **2013**, *10*, 176–187. [CrossRef]
52. Estrada, E.; Labat, M.; Lorente, S.; Rocha, L.A.O. The Impact of Latent Heat Exchanges on the Design of Earth Air Heat Exchangers. *Appl. Therm. Eng.* **2018**, *129*, 306–317. [CrossRef]
53. Zhou, T.; Xiao, Y.; Liu, Y.; Lin, J.; Huang, H. Research on Cooling Performance of Phase Change Material-Filled Earth-Air Heat Exchanger. *Energy Convers. Manag.* **2018**, *177*, 210–223. [CrossRef]
54. Liu, Z.; Yu, Z.; Yang, T.; El Mankibi, M.; Roccamena, L.; Sun, Y.; Sun, P.; Li, S.; Zhang, G. Experimental and Numerical Study of a Vertical Earth-to-Air Heat Exchanger System Integrated with Annular Phase Change Material. *Energy Convers. Manag.* **2019**, *186*, 433–449. [CrossRef]
55. Yang, D.; Shi, R.; Wei, H.; Du, J.; Wang, J. Investigation of the Performance of a Cylindrical PCM-to-Air Heat Exchanger (PAHE) for Free Ventilation Cooling in Fluctuating Ambient Environments. *Sustain. Cities Soc.* **2019**, *51*, 101764. [CrossRef]

56. Zhou, T.; Xiao, Y.; Huang, H.; Lin, J. Numerical Study on the Cooling Performance of a Novel Passive System: Cylindrical Phase Change Material-Assisted Earth-Air Heat Exchanger. *J. Clean. Prod.* **2020**, *245*, 118907. [CrossRef]
57. Lu, S.; Liang, B.; Li, X.; Kong, X.; Jia, W.; Wang, L. Performance Analysis of PCM Ceiling Coupling with Earth-Air Heat Exchanger for Building Cooling. *Materials* **2020**, *13*, 2890. [CrossRef] [PubMed]
58. Qin, D.; Liu, J.; Zhang, G. A Novel Solar-Geothermal System Integrated with Earth–to–Air Heat Exchanger and Solar Air Heater with Phase Change Material—Numerical Modelling, Experimental Calibration and Parametrical Analysis. *J. Build. Eng.* **2021**, *35*, 101971. [CrossRef]
59. Qin, D.; Liu, Z.; Zhou, Y.; Yan, Z.; Chen, D.; Zhang, G. Dynamic Performance of a Novel Air-Soil Heat Exchanger Coupling with Diversified Energy Storage Components—Modelling Development, Experimental Verification, Parametrical Design and Robust Operation. *Renew. Energy* **2020**, *167*, 542–557. [CrossRef]
60. Liu, Q.; Huang, Y.; Ma, Y.; Peng, Y.; Wang, Y. Parametric Study on the Thermal Performance of Phase Change Material-Assisted Earth-to-Air Heat Exchanger. *Energy Build.* **2021**, *238*, 110811. [CrossRef]
61. Liu, Z.; Sun, P.; Xie, M.; Zhou, Y.; He, Y.; Zhang, G.; Chen, D.; Li, S.; Yan, Z.; Qin, D. Multivariant Optimization and Sensitivity Analysis of an Experimental Vertical Earth-to-Air Heat Exchanger System Integrating Phase Change Material with Taguchi Method. *Renew. Energy* **2021**, *173*, 401–414. [CrossRef]
62. Maytorena, V.M.; Moreno, S.; Hinojosa, J.F. Effect of Operation Modes on the Thermal Performance of EAHE Systems with and without PCM in Summer Weather Conditions. *Energy Build.* **2021**, *250*, 111278. [CrossRef]
63. Long, T.; Li, W.; Lv, Y.; Li, Y.; Liu, S.; Lu, J.; Huang, S.; Zhang, Y. Benefits of Integrating Phase-Change Material with Solar Chimney and Earth-to-Air Heat Exchanger System for Passive Ventilation and Cooling in Summer. *J. Energy Storage* **2022**, *48*, 104037. [CrossRef]
64. Ouzzane, M.; Bady, M. Investigation of an Innovative Canadian Well System Combined with a Frozen Water/PCM Heat Exchanger for Air-Cooling in Hot Climate. *Appl. Therm. Eng.* **2022**, *213*, 118737. [CrossRef]
65. Guo, X.; Wei, H.; He, X.; He, M.; Yang, D. Integrating Phase Change Material in Building Envelopes Combined with the Earth-to-Air Heat Exchanger for Indoor Thermal Environment Regulation. *Build. Environ.* **2022**, *221*, 109318. [CrossRef]
66. Maytorena, V.M.; Hinojosa, J.F.; Moreno, S.; Buentello-Montoya, D.A. Thermal Performance Analysis of a Passive Hybrid Earth-to-Air Heat Exchanger for Cooling Rooms at Mexican Desert Climate. *Case Stud. Therm. Eng.* **2023**, *41*, 102590. [CrossRef]
67. Durakovic, B.; Torlak, M. Experimental and Numerical Study of a PCM Window Model as a Thermal Energy Storage Unit. *Int. J. Low-Carbon Technol.* **2016**, *12*, 272–280. [CrossRef]
68. Duraković, B.; Mešetović, S. Thermal Performances of Glazed Energy Storage Systems with Various Storage Materials: An Experimental Study. *Sustain. Cities Soc.* **2019**, *45*, 422–430. [CrossRef]
69. Zhang, S.; Ma, Y.; Li, D.; Liu, C.; Yang, R. Thermal Performance of a Reversible Multiple-Glazing Roof Filled with Two PCM. *Renew. Energy* **2022**, *182*, 1080–1093. [CrossRef]
70. Li, D.; Ma, Y.; Zhang, S.; Yang, R.; Zhang, C.; Liu, C. Photothermal and Energy Performance of an Innovative Roof Based on Silica Aerogel-PCM Glazing Systems. *Energy Convers. Manag.* **2022**, *262*, 115567. [CrossRef]
71. Wang, S.; Zhang, C.; Zhang, S.; Zhou, Y.; Arıcı, M. Characteristics of PCMs-Filled Double Glazing Unit under Fire: A Detailed Thermal Structural Analysis. *J. Build. Eng.* **2023**, *65*, 105672. [CrossRef]
72. Wang, D.; Liu, H.; Liu, Y.; Xu, T.; Wang, Y.; Du, H.; Wang, X.; Liu, J. Frost and High-Temperature Resistance Performance of a Novel Dual-Phase Change Material Flat Plate Solar Collector. *Sol. Energy Mater. Sol. Cells* **2019**, *201*, 110086. [CrossRef]
73. Abuşka, M.; Şevik, S.; Kayapunar, A. Experimental Analysis of Solar Air Collector with PCM-Honeycomb Combination under the Natural Convection. *Sol. Energy Mater. Sol. Cells* **2019**, *195*, 299–308. [CrossRef]
74. Charvát, P.; Klimeš, L.; Pech, O.; Hejčík, J. Solar Air Collector with the Solar Absorber Plate Containing a PCM—Environmental Chamber Experiments and Computer Simulations. *Renew. Energy* **2019**, *143*, 731–740. [CrossRef]
75. Palacio, M.; Rincón, A.; Carmona, M. Experimental Comparative Analysis of a Flat Plate Solar Collector with and without PCM. *Sol. Energy* **2020**, *206*, 708–721. [CrossRef]
76. Benkaddour, A.; Faraji, M.; Faraji, H. Numerical Study of the Thermal Energy Storage Behaviour of a Novel Composite PCM/Concrete Wall Integrated Solar Collector. *Mater. Today Proc.* **2020**, *30*, 905–908. [CrossRef]
77. Aramesh, M.; Shabani, B. On the Integration of Phase Change Materials with Evacuated Tube Solar Thermal Collectors. *Renew. Sustain. Energy Rev.* **2020**, *132*, 110135. [CrossRef]
78. Chopra, K.; Tyagi, V.V.; Pandey, A.K.; Sharma, R.K.; Sari, A. PCM Integrated Glass in Glass Tube Solar Collector for Low and Medium Temperature Applications: Thermodynamic & Techno-Economic Approach. *Energy* **2020**, *198*, 117238. [CrossRef]
79. Abu-Arabi, M.; Al-harahsheh, M.; Ahmad, M.; Mousa, H. Theoretical Modeling of a Glass-Cooled Solar Still Incorporating PCM and Coupled to Flat Plate Solar Collector. *J. Energy Storage* **2020**, *29*, 101372. [CrossRef]
80. Bejan, A.S.; Teodosiu, C.; Croitoru, C.V.; Catalina, T.; Nastase, I. Experimental Investigation of Transpired Solar Collectors with/without Phase Change Materials. *Sol. Energy* **2021**, *214*, 478–490. [CrossRef]
81. Ebrahimi, H.; Akhijahani, H.S.; Salami, P. Improving the Thermal Efficiency of a Solar Dryer Using Phase Change Materials at Different Position in the Collector. *Sol. Energy* **2021**, *220*, 535–551. [CrossRef]
82. Elarem, R.; Alqahtani, T.; Mellouli, S.; Aich, W.; Ben Khedher, N.; Kolsi, L.; Jemni, A. Numerical Study of an Evacuated Tube Solar Collector Incorporating a Nano-PCM as a Latent Heat Storage System. *Case Stud. Therm. Eng.* **2021**, *24*, 100859. [CrossRef]

83. Thakur, A.; Kumar, R.; Kumar, S.; Kumar, P. Review of Developments on Flat Plate Solar Collectors for Heat Transfer Enhancements Using Phase Change Materials and Reflectors. *Mater. Today Proc.* **2021**, *45*, 5449–5455. [CrossRef]
84. Wheatley, G.; Rubel, R.I. Design Improvement of a Laboratory Prototype for Efficiency Evaluation of Solar Thermal Water Heating System Using Phase Change Material (PCMs). *Results Eng.* **2021**, *12*, 100301. [CrossRef]
85. Assadeg, J.; Al-Waeli, A.H.A.; Fudholi, A.; Sopian, K. Energetic and Exergetic Analysis of a New Double Pass Solar Air Collector with Fins and Phase Change Material. *Sol. Energy* **2021**, *226*, 260–271. [CrossRef]
86. Zhang, T.; Lu, G.; Zhai, X.; Li, B. Structure Optimization of a Phase Change Material Integrated Solar Air Collector/Storage Unit Based upon Phase Change Analysis. *Energy Rep.* **2021**, *7*, 1828–1836. [CrossRef]
87. Luo, Q.; Li, B.; Wang, Z.; Su, S.; Xiao, H.; Zhu, C. Thermal Modeling of Air-Type Double-Pass Solar Collector with PCM-Rod Embedded in Vacuum Tube. *Energy Convers. Manag.* **2021**, *235*, 113952. [CrossRef]
88. Alshukri, M.J.; Eidan, A.A.; Najim, S.I. Thermal Performance of Heat Pipe Evacuated Tube Solar Collector Integrated with Different Types of Phase Change Materials at Various Location. *Renew. Energy* **2021**, *171*, 635–646. [CrossRef]
89. Nawsud, Z.A.; Altouni, A.; Akhijahani, H.S.; Kargarsharifabad, H. A Comprehensive Review on the Use of Nano-Fluids and Nano-PCM in Parabolic Trough Solar Collectors (PTC). *Sustain. Energy Technol. Assess.* **2022**, *51*, 101889. [CrossRef]
90. Li, J.; Zhang, W.; Xie, L.; Li, Z.; Wu, X.; Zhao, O.; Zhong, J.; Zeng, X. A Hybrid Photovoltaic and Water/Air Based Thermal(PVT) Solar Energy Collector with Integrated PCM for Building Application. *Renew. Energy* **2022**, *199*, 662–671. [CrossRef]
91. Feng, L.; Liu, J.; Lu, H.; Chen, Y.; Wu, S. A Parametric Study on the Efficiency of a Solar Evacuated Tube Collector Using Phase Change Materials: A Transient Simulation. *Renew. Energy* **2022**, *199*, 745–758. [CrossRef]
92. Wang, D.; Huo, X.; Liu, Y.; Chen, Y.; Fan, B.; Xu, T.; Wang, L. A Study on Frost and High-Temperature Resistance Performance of Supercooled Phase Change Material-Based Flat Panel Solar Collector. *Sol. Energy Mater. Sol. Cells* **2022**, *239*, 111665. [CrossRef]
93. Peralta, I.; Fachinotti, V.D.; Koenders, E.A.B.; Caggiano, A. Computational Design of a Massive Solar-Thermal Collector Enhanced with Phase Change Materials. *Energy Build.* **2022**, *274*, 112437. [CrossRef]
94. Palacio, M.; Ramírez, C.; Carmona, M.; Cortés, C. Effect of Phase-Change Materials in the Performance of a Solar Air Heater. *Sol. Energy* **2022**, *247*, 385–396. [CrossRef]
95. Alqaed, S. Effect of Using a Solar Hot Air Collector Installed on the Inclined Roof of a Building for Cooling and Heating System in the Presence of Polymeric PCM. *Sustain. Energy Technol. Assess.* **2022**, *50*, 101852. [CrossRef]
96. Wu, Y.; Tong, X.; Li, D.; Arıcı, M.; Liu, C.; Liu, Y.; Yang, R.; Yu, Y. Energy Analysis of Evacuated Tube Solar Collector Integrating Phase Change Material in Northeast China. *J. Energy Storage* **2022**, *55*, 105772. [CrossRef]
97. Sadeghi, G.; Mehrali, M.; Shahi, M.; Brem, G.; Mahmoudi, A. Experimental Analysis of Shape-Stabilized PCM Applied to a Direct-Absorption Evacuated Tube Solar Collector Exploiting Sodium Acetate Trihydrate and Graphite. *Energy Convers. Manag.* **2022**, *269*, 116176. [CrossRef]
98. Yeh, C.-Y.; Boonk, K.J.F.; Sadeghi, G.; Mehrali, M.; Shahi, M.; Brem, G.; Mahmoudi, A. Experimental and Numerical Analysis of Thermal Performance of Shape Stabilized PCM in a Solar Thermal Collector. *Case Stud. Therm. Eng.* **2022**, *30*, 101706. [CrossRef]
99. Bejan, A.-S.; Croitoru, C.; Bode, F.; Teodosiu, C.; Catalina, T. Experimental Investigation of an Enhanced Transpired Air Solar Collector with Embodied Phase Changing Materials. *J. Clean. Prod.* **2022**, *336*, 130398. [CrossRef]
100. Bouadila, S.; Baddadi, S.; Rehman, T.; Ayed, R. Experimental Investigation on the Thermal Appraisal of Heat Pipe-Evacuated Tube Collector-Based Water Heating System Integrated with PCM. *Renew. Energy* **2022**, *199*, 382–394. [CrossRef]
101. Dinesh, S.; Saminathan, R.; Patil, M.M.; Baviskar, P.R.; Hadidi, H.; Vignesh, S.; Kumar, P.M. Investigating the Single Pass Baffled Solar Air Heater (SAH) with an Organic PCM (OPCM). *Mater. Today Proc.* **2022**, *62*, 5245–5249. [CrossRef]
102. Nekoonam, S.; Ghasempour, R. Modeling and Optimization of a Thermal Energy Storage Unit with Cascaded PCM Capsules in Connection to a Solar Collector. *Sustain. Energy Technol. Assess.* **2022**, *52*, 102197. [CrossRef]
103. Olfian, H.; Ajarostaghi, S.S.M.; Ebrahimnataj, M.; Farhadi, M.; Arıcı, M. On the Thermal Performance of Evacuated Tube Solar Collector Integrated with Phase Change Material. *Sustain. Energy Technol. Assess.* **2022**, *53*, 102437. [CrossRef]
104. Li, Y.; Liang, X.; Song, W.; Li, T.; Wang, D.; Liu, Y. Optimization and Thermal Performance of U-Type Evacuated Tube Solar Collector Filled with Phase Change Material. *Energy Rep.* **2022**, *8*, 6126–6138. [CrossRef]
105. Sadeghi, G.; Mehrali, M.; Shahi, M.; Brem, G.; Mahmoudi, A. Progress of Experimental Studies on Compact Integrated Solar Collector-Storage Retrofits Adopting Phase Change Materials. *Sol. Energy* **2022**, *237*, 62–95. [CrossRef]
106. Sethi, M.; Tripathi, R.K.; Pattnaik, B.; Kumar, S.; Khargotra, R.; Chand, S.; Thakur, A. Recent Developments in Design of Evacuated Tube Solar Collectors Integrated with Thermal Energy Storage: A Review. *Mater. Today Proc.* **2022**, *52*, 1689–1696. [CrossRef]
107. He, Z.; Ma, H.; Lu, S.; Sun, Y. Research on the Thermal Performance of Interlayer Ventilated PCM Component Coupled with Solar Air Collector. *Energy Build.* **2022**, *255*, 111698. [CrossRef]
108. Abu-Hamdeh, N.H.; Khoshaim, A.; Alzahrani, M.A.; Hatamleh, R.I. Sustainable and Renewable Energy Management by Investigating the Effect of the Diameter of Finned Tubes of a Solar Collector on Its Heat Production in the Presence of Phase Change Materials in a Residential Building. *J. Build. Eng.* **2022**, *57*, 104881. [CrossRef]
109. Hatamleh, R.I.; Abu-Hamdeh, N.H.; Khoshaim, A.; Alzahrani, M.A. Using Phase Change Material (PCM) to Improve the Solar Energy Capacity of Glass in Solar Collectors by Enhancing Their Thermal Performance via Developed MD Approach. *Eng. Anal. Bound. Elem.* **2022**, *143*, 163–169. [CrossRef]
110. Preet, S.; Bhushan, B.; Mahajan, T. Experimental Investigation of Water Based Photovoltaic/Thermal (PV/T) System with and without Phase Change Material (PCM). *Sol. Energy* **2017**, *155*, 1104–1120. [CrossRef]

111. Al-Waeli, A.H.A.; Sopian, K.; Kazem, H.A.; Yousif, J.H.; Chaichan, M.T.; Ibrahim, A.; Mat, S.; Ruslan, M.H. Comparison of Prediction Methods of PV/T Nanofluid and Nano-PCM System Using a Measured Dataset and Artificial Neural Network. *Sol. Energy* **2018**, *162*, 378–396. [CrossRef]
112. Nada, S.A.; El-Nagar, D.H.; Hussein, H.M.S. Improving the Thermal Regulation and Efficiency Enhancement of PCM-Integrated PV Modules Using Nano Particles. *Energy Convers. Manag.* **2018**, *166*, 735–743. [CrossRef]
113. Khanna, S.; Reddy, K.S.; Mallick, T.K. Optimization of Finned Solar Photovoltaic Phase Change Material (Finned Pv Pcm) System. *Int. J. Therm. Sci.* **2018**, *130*, 313–322. [CrossRef]
114. Darkwa, J.; Calautit, J.; Du, D.; Kokogianakis, G. A Numerical and Experimental Analysis of an Integrated TEG-PCM Power Enhancement System for Photovoltaic Cells. *Appl. Energy* **2019**, *248*, 688–701. [CrossRef]
115. Maatallah, T.; Zachariah, R.; Al-Amri, F.G. Exergo-Economic Analysis of a Serpentine Flow Type Water Based Photovoltaic Thermal System with Phase Change Material (PVT-PCM/Water). *Sol. Energy* **2019**, *193*, 195–204. [CrossRef]
116. Rajvikram, M.; Leoponraj, S.; Ramkumar, S.; Akshaya, H.; Dheeraj, A. Experimental Investigation on the Abasement of Operating Temperature in Solar Photovoltaic Panel Using PCM and Aluminium. *Sol. Energy* **2019**, *188*, 327–338. [CrossRef]
117. Siahkamari, L.; Rahimi, M.; Azimi, N.; Banibayat, M. Experimental Investigation on Using a Novel Phase Change Material (PCM) in Micro Structure Photovoltaic Cooling System. *Int. Commun. Heat Mass Transf.* **2019**, *100*, 60–66. [CrossRef]
118. Soares, N.; Costa, J.J.; Gaspar, A.R.; Matias, T.; Simões, P.N.; Durães, L. Can Movable PCM-Filled TES Units Be Used to Improve the Performance of PV Panels? Overview and Experimental Case-Study. *Energy Build.* **2020**, *210*, 109743. [CrossRef]
119. Kumar, A.; Singh, A.P.; Singh, O.P. Effect of Novel PCM Encapsulation Designs on Electrical and Thermal Performance of a Hybrid Photovoltaic Solar Panel. *Sol. Energy* **2020**, *205*, 320–333. [CrossRef]
120. Savvakis, N.; Dialyna, E.; Tsoutsos, T. Investigation of the Operational Performance and Efficiency of an Alternative PV + PCM Concept. *Sol. Energy* **2020**, *211*, 1283–1300. [CrossRef]
121. Elsheniti, M.B.; Hemedah, M.A.; Sorour, M.M.; El-Maghlany, W.M. Novel Enhanced Conduction Model for Predicting Performance of a PV Panel Cooled by PCM. *Energy Convers. Manag.* **2020**, *205*, 112456. [CrossRef]
122. Abdollahi, N.; Rahimi, M. Potential of Water Natural Circulation Coupled with Nano-Enhanced PCM for PV Module Cooling. *Renew. Energy* **2020**, *147*, 302–309. [CrossRef]
123. Mahdi, J.M.; Mohammed, H.I.; Talebizadehsardari, P. A New Approach for Employing Multiple PCMs in the Passive Thermal Management of Photovoltaic Modules. *Sol. Energy* **2021**, *222*, 160–174. [CrossRef]
124. Singh, A.P.; Kumar, A.; Singh, O.P. Effect of Natural Convection and Thermal Storage System on the Electrical and Thermal Performance of a Hybrid PV-T/PCM Systems. *Mater. Today Proc.* **2021**, *39*, 1899–1904. [CrossRef]
125. Xu, H.; Wang, N.; Zhang, C.; Qu, Z.; Karimi, F. Energy Conversion Performance of a PV/T-PCM System under Different Thermal Regulation Strategies. *Energy Convers. Manag.* **2021**, *229*, 113660. [CrossRef]
126. Kumar, K.S.; Kumar, H.A.; Gowtham, P.; Kumar, S.H.S.; Sudhan, R.H. Experimental Analysis and Increasing the Energy Efficiency of PV Cell with Nano-PCM (Calcium Carbonate, Silicon Carbide, Copper). *Mater. Today Proc.* **2021**, *37*, 1221–1225. [CrossRef]
127. Carmona, M.; Bastos, A.P.; García, J.D. Experimental Evaluation of a Hybrid Photovoltaic and Thermal Solar Energy Collector with Integrated Phase Change Material (PVT-PCM) in Comparison with a Traditional Photovoltaic (PV) Module. *Renew. Energy* **2021**, *172*, 680–696. [CrossRef]
128. Abdulmunem, A.; Samin, P.M.; Rahman, H.A.; Hussien, H.; Mazali, I.I.; Ghazali, H. Numerical and Experimental Analysis of the Tilt Angle's Effects on the Characteristics of the Melting Process of PCM-Based as PV Cell's Backside Heat Sink. *Renew. Energy* **2021**, *173*, 520–530. [CrossRef]
129. Sudhakar, P.; Santosh, R.; Asthalakshmi, B.; Kumaresan, G.; Velraj, R. Performance Augmentation of Solar Photovoltaic Panel through PCM Integrated Natural Water Circulation Cooling Technique. *Renew. Energy* **2021**, *172*, 1433–1448. [CrossRef]
130. Rahmanian, S.; Moein-Jahromi, M.; Rahmanian-Koushkaki, H.; Sopian, K. Performance Investigation of Inclined CPV System with Composites of PCM, Metal Foam and Nanoparticles. *Sol. Energy* **2021**, *230*, 883–901. [CrossRef]
131. Savvakis, N.; Tsoutsos, T. Theoretical Design and Experimental Evaluation of a PV+PCM System in the Mediterranean Climate. *Energy* **2021**, *220*, 119690. [CrossRef]
132. Duan, J. The PCM-Porous System Used to Cool the Inclined PV Panel. *Renew. Energy* **2021**, *180*, 1315–1332. [CrossRef]
133. Kumar, A.; Singh, A.P.; Kotha, R.S.; Singh, O. Thermal Energy Storage Design of a New Bifacial PV/PCM System for Enhanced Thermo-Electric Performance. *Energy Convers. Manag.* **2021**, *250*, 114912. [CrossRef]
134. Özbaş, E. A Novel Design of Passive Cooler for PV with PCM and Two-Phase Closed Thermosyphons. *Sol. Energy* **2022**, *245*, 19–24. [CrossRef]
135. Soliman, A.S.; Xu, L.; Dong, J.; Cheng, P. A Novel Heat Sink for Cooling Photovoltaic Systems Using Convex/Concave Dimples and Multiple PCMs. *Appl. Therm. Eng.* **2022**, *215*, 119001. [CrossRef]
136. Díaz, F.A.; Moraga, N.O.; Cabrales, R.C. Computational Modeling of a PV-PCM Passive Cooling System during a Day–Night Cycle at Arid and Semi-Arid Climate Zones. *Energy Convers. Manag.* **2022**, *270*, 116202. [CrossRef]
137. Cui, Y.; Zhu, J.; Zhang, F.; Shao, Y.; Xue, Y. Current Status and Future Development of Hybrid PV/T System with PCM Module: 4E (Energy, Exergy, Economic and Environmental) Assessments. *Renew. Sustain. Energy Rev.* **2022**, *158*, 112147. [CrossRef]
138. Gad, R.; Mahmoud, H.; Ookawara, S.; Hassan, H. Energy, Exergy, and Economic Assessment of Thermal Regulation of PV Panel Using Hybrid Heat Pipe-Phase Change Material Cooling System. *J. Clean. Prod.* **2022**, *364*, 132489. [CrossRef]

139. Kouravand, A.; Kasaeian, A.; Pourfayaz, F.; Rad, M.A.V. Evaluation of a Nanofluid-Based Concentrating Photovoltaic Thermal System Integrated with Finned PCM Heatsink: An Experimental Study. *Renew. Energy* **2022**, *201*, 1010–1025. [CrossRef]
140. Moein-Jahromi, M.; Rahmanian-Koushkaki, H.; Rahmanian, S.; Jahromi, S.P. Evaluation of Nanostructured GNP and CuO Compositions in PCM-Based Heat Sinks for Photovoltaic Systems. *J. Energy Storage* **2022**, *53*, 105240. [CrossRef]
141. Nasef, H.A.; Hassan, H.; Mori, S.; Nada, S.A. Experimental Investigation on the Performance of Parallel and Staggered Arrays of PCM Energy Storage System for PV Thermal Regulation. *Energy Convers. Manag.* **2022**, *254*, 115143. [CrossRef]
142. Bhakre, S.S.; Sawarkar, P.D.; Kalamkar, V.R. Experimental Study on Photovoltaic Panel Integrated with Polyethylene Glycol 1500 Phase Change Material. *J. Energy Storage* **2022**, *55*, 105518. [CrossRef]
143. Kong, X.; Zhang, L.; Li, H.; Wang, Y.; Fan, M. Experimental Thermal and Electrical Performance Analysis of a Concentrating Photovoltaic/Thermal System Integrated with Phase Change Material (PV/T-CPCM). *Sol. Energy Mater. Sol. Cells* **2022**, *234*, 111415. [CrossRef]
144. Colarossi, D.; Tagliolini, E.; Amato, A.; Principi, P. Life Cycle Assessment and Circularity Evaluation of a PV Panel Integrated with Phase Change Material. *Renew. Energy* **2022**, *201*, 150–156. [CrossRef]
145. Al-Najjar, H.M.T.; Mahdi, J.M. Novel Mathematical Modeling, Performance Analysis, and Design Charts for the Typical Hybrid Photovoltaic/Phase-Change Material (PV/PCM) System. *Appl. Energy* **2022**, *315*, 119027. [CrossRef]
146. Azimi, N.; Davoodbeygi, Y.; Rahimi, M.; Ahmadi, S.; Karami, E.; Roshani, M. Optimization of Thermal and Electrical Efficiencies of a Photovoltaic Module Using Combined PCMs with a Thermo-Conductive Filler. *Sol. Energy* **2022**, *231*, 283–296. [CrossRef]
147. Ben Zohra, M.; Riad, A.; Alhamany, A. Optimizing the Conception of Hybrid PV/PCM by Optimizing the Heat Transfer at the Contact Interface and by Integrating Two Types of PCM. *Results Eng.* **2022**, *16*, 100614. [CrossRef]
148. Wen, X.; Ji, J.; Li, Z.; Song, Z. Performance Analysis of a Concentrated System with Series Photovoltaic/Thermal Module and Solar Thermal Collector Integrated with PCM and TEG. *Energy* **2022**, *249*, 123777. [CrossRef]
149. Xiao, Y.; Huang, P.; Wei, G.; Cui, L.; Xu, C.; Du, X. State-of-the-Art Review on Performance Enhancement of Photovoltaic/Thermal System Integrated with Phase Change Materials. *J. Energy Storage* **2022**, *56*, 106073. [CrossRef]
150. Luo, Z.; Zhu, N.; Hu, P.; Lei, F.; Zhang, Y. Simulation Study on Performance of PV-PCM-TE System for Year-Round Analysis. *Renew. Energy* **2022**, *195*, 263–273. [CrossRef]
151. He, Y.; Tao, Y.B.; Zhao, C.Y.; Yu, X.K. Structure Parameter Analysis and Optimization of Photovoltaic-Phase Change Material-Thermoelectric Coupling System under Space Conditions. *Renew. Energy* **2022**, *200*, 320–333. [CrossRef]
152. Amalu, E.H.; Fabunmi, O.A. Thermal Control of Crystalline Silicon Photovoltaic (c-Si PV) Module Using Docosane Phase Change Material (PCM) for Improved Performance. *Sol. Energy* **2022**, *234*, 203–221. [CrossRef]
153. Gao, Y.; Dai, Z.; Wu, D.; Wang, C.; Chen, B.; Zhang, X. Transient Performance Assessment of a Hybrid PV-TEG System Integrated with PCM under Non-Uniform Radiation Conditions: A Numerical Investigation. *Renew. Energy* **2022**, *198*, 352–366. [CrossRef]
154. Colarossi, D.; Principi, P. Yearly Performance of a PV-PCM and Water Storage for Domestic Hot Water Energy Demand. *Energy Build.* **2022**, *274*, 112451. [CrossRef]
155. Li, S.; Peng, J.; Li, H.; Zou, B.; Song, J.; Ma, T.; Ji, J. Zero Energy Potential of PV Direct-Driven Air Conditioners Coupled with Phase Change Materials and Load Flexibility. *Renew. Energy* **2022**, *200*, 419–432. [CrossRef]
156. Homlakorn, S.; Suksri, A.; Wongwuttanasatian, T. Efficiency Improvement of PV Module Using a Binary-Organic Eutectic Phase Change Material in a Finned Container. *Energy Rep.* **2022**, *8*, 121–128. [CrossRef]
157. Bria, A.; Raillani, B.; Chaatouf, D.; Salhi, M.; Amraqui, S.; Mezrhab, A. Effect of PCM Thickness on the Performance of the Finned PV/PCM System. *Mater. Today Proc.* **2023**, *72*, 3617–3625. [CrossRef]
158. Foteinis, S.; Savvakis, N.; Tsoutsos, T. Energy and Environmental Performance of Photovoltaic Cooling Using Phase Change Materials under the Mediterranean Climate. *Energy* **2023**, *265*, 126355. [CrossRef]
159. Lv, S.; Yang, J.; Ren, J.; Zhang, B.; Lai, Y.; Chang, Z. Research and Numerical Analysis on Performance Optimization of Photovoltaic-Thermoelectric System Incorporated with Phase Change Materials. *Energy* **2023**, *263*, 125850. [CrossRef]
160. Zhang, C.; Wang, N.; Xu, H.; Fang, Y.; Yang, Q.; Talkhoncheh, F.K. Thermal Management Optimization of the Photovoltaic Cell by the Phase Change Material Combined with Metal Fins. *Energy* **2023**, *263*, 125669. [CrossRef]
161. Sarhaddi, F.; Tabrizi, F.F.; Zoori, H.A.; Mousavi, S.A.H.S. Comparative Study of Two Weir Type Cascade Solar Stills with and without PCM Storage Using Energy and Exergy Analysis. *Energy Convers. Manag.* **2017**, *133*, 97–109. [CrossRef]
162. Arunkumar, T.; Kabeel, A.E. Effect of Phase Change Material on Concentric Circular Tubular Solar Still-Integration Meets Enhancement. *Desalination* **2017**, *414*, 46–50. [CrossRef]
163. Faegh, M.; Shafii, M.B. Experimental Investigation of a Solar Still Equipped with an External Heat Storage System Using Phase Change Materials and Heat Pipes. *Desalination* **2017**, *409*, 128–135. [CrossRef]
164. Kabeel, A.E.; Abdelgaied, M. Observational Study of Modified Solar Still Coupled with Oil Serpentine Loop from Cylindrical Parabolic Concentrator and Phase Changing Material under Basin. *Sol. Energy* **2017**, *144*, 71–78. [CrossRef]
165. Kabeel, A.; Elkelawy, M.; El Din, H.A.; Alghrubah, A. Investigation of Exergy and Yield of a Passive Solar Water Desalination System with a Parabolic Concentrator Incorporated with Latent Heat Storage Medium. *Energy Convers. Manag.* **2017**, *145*, 10–19. [CrossRef]
166. Sharshir, S.W.; Peng, G.; Wu, L.; Essa, F.A.; Kabeel, A.E.; Yang, N. The Effects of Flake Graphite Nanoparticles, Phase Change Material, and Film Cooling on the Solar Still Performance. *Appl. Energy* **2017**, *191*, 358–366. [CrossRef]

167. Al-harahsheh, M.; Abu-Arabi, M.; Mousa, H.; Alzghoul, Z. Solar Desalination Using Solar Still Enhanced by External Solar Collector and PCM. *Appl. Therm. Eng.* **2018**, *128*, 1030–1040. [CrossRef]
168. Mazraeh, A.E.; Babayan, M.; Yari, M.; Sefidan, A.M.; Saha, S.C. Theoretical Study on the Performance of a Solar Still System Integrated with PCM-PV Module for Sustainable Water and Power Generation. *Desalination* **2018**, *443*, 184–197. [CrossRef]
169. Abu-Arabi, M.; Al-harahsheh, M.; Mousa, H.; Alzghoul, Z. Theoretical Investigation of Solar Desalination with Solar Still Having Phase Change Material and Connected to a Solar Collector. *Desalination* **2018**, *448*, 60–68. [CrossRef]
170. Rufuss, D.D.W.; Suganthi, L.; Iniyan, S.; Davies, P. Effects of Nanoparticle-Enhanced Phase Change Material (NPCM) on Solar Still Productivity. *J. Clean. Prod.* **2018**, *192*, 9–29. [CrossRef]
171. Elbar, A.R.A.; Hassan, H. Experimental Investigation on the Impact of Thermal Energy Storage on the Solar Still Performance Coupled with PV Module via New Integration. *Sol. Energy* **2019**, *184*, 584–593. [CrossRef]
172. Safaei, M.R.; Goshayeshi, H.R.; Chaer, I. Solar Still Efficiency Enhancement by Using Graphene Oxide/Paraffin Nano-PCM. *Energies* **2019**, *12*, 2002. [CrossRef]
173. Kumbhar, S.V. Double Slope Solar Still Distillate Output Data Set for Conventional Still and Still with or without Reflectors and PCM Using High TDS Water Samples. *Data Brief* **2019**, *24*, 103852. [CrossRef]
174. Vigneswaran, V.S.; Kumaresan, G.; Dinakar, B.V.; Kamal, K.K.; Velraj, R. Augmenting the Productivity of Solar Still Using Multiple PCMs as Heat Energy Storage. *J. Energy Storage* **2019**, *26*, 101019. [CrossRef]
175. Cheng, W.L.; Huo, Y.K.; Nian, Y. Le Performance of Solar Still Using Shape-Stabilized PCM: Experimental and Theoretical Investigation. *Desalination* **2019**, *455*, 89–99. [CrossRef]
176. Mousa, H.; Naser, J.; Gujarathi, A.M.; Al-Sawafi, S. Experimental Study and Analysis of Solar Still Desalination Using Phase Change Materials. *J. Energy Storage* **2019**, *26*, 100959. [CrossRef]
177. Yousef, M.S.; Hassan, H.; Kodama, S.; Sekiguchi, H. An Experimental Study on the Performance of Single Slope Solar Still Integrated with a PCM-Based Pin-Finned Heat Sink. *Energy Procedia* **2019**, *156*, 100–104. [CrossRef]
178. Dawood, M.M.K.; Nabil, T.; Kabeel, A.; Shehata, A.I.; Abdalla, A.M.; Elnaghi, B.E. Experimental Study of Productivity Progress for a Solar Still Integrated with Parabolic Trough Collectors with a Phase Change Material in the Receiver Evacuated Tubes and in the Still. *J. Energy Storage* **2020**, *32*, 102007. [CrossRef]
179. Kabeel, A.E.; Sathyamurthy, R.; Manokar, A.M.; Sharshir, S.W.; Essa, F.A.; Elshiekh, A.H. Experimental Study on Tubular Solar Still Using Graphene Oxide Nano Particles in Phase Change Material (NPCM's) for Fresh Water Production. *J. Energy Storage* **2020**, *28*, 101204. [CrossRef]
180. Kabeel, A.E.; Abdelgaied, M.; Harby, K.; Eisa, A. Augmentation of Diurnal and Nocturnal Distillate of Modified Tubular Solar Still Having Copper Tubes Filled with PCM in the Basin. *J. Energy Storage* **2020**, *32*, 101992. [CrossRef]
181. Thalib, M.M.; Manokar, A.M.; Essa, F.A.; Vasimalai, N.; Sathyamurthy, R.; Garcia Marquez, F.P. Comparative Study of Tubular Solar Stills with Phase Change Material and Nano-Enhanced Phase Change Material. *Energies* **2020**, *13*, 3989. [CrossRef]
182. Kabeel, A.E.; El-Maghlany, W.M.; Abdelgaied, M.; Abdel-Aziz, M.M. Performance Enhancement of Pyramid-Shaped Solar Stills Using Hollow Circular Fins and Phase Change Materials. *J. Energy Storage* **2020**, *31*, 101610. [CrossRef]
183. Ghadamgahi, M.; Ahmadi-Danesh-Ashtiani, H.; Delfani, S. Comparative Study on the Multistage Solar Still Performance Utilizing PCM in Variable Thicknesses. *Int. J. Energy Res.* **2020**, *44*, 4196–4210. [CrossRef]
184. Hedayati-Mehdiabadi, E.; Sarhaddi, F.; Sobhnamayan, F. Exergy Performance Evaluation of a Basin-Type Double-Slope Solar Still Equipped with Phase-Change Material and PV/T Collector. *Renew. Energy* **2020**, *145*, 2409–2425. [CrossRef]
185. Hafs, H.; Asbik, M.; Boushaba, H.; Koukouch, A.; Zaaoumi, A.; Bah, A.; Ansari, O. Numerical Simulation of the Performance of Passive and Active Solar Still with Corrugated Absorber Surface as Heat Storage Medium for Sustainable Solar Desalination Technology. *Groundw. Sustain. Dev.* **2021**, *14*, 100610. [CrossRef]
186. Abdullah, A.S.; Omara, Z.M.; Essa, F.A.; Younes, M.M.; Shanmugan, S.; Abdelgaied, M.; Amro, M.I.; Kabeel, A.E.; Farouk, W.M. Improving the Performance of Trays Solar Still Using Wick Corrugated Absorber, Nano-Enhanced Phase Change Material and Photovoltaics-Powered Heaters. *J. Energy Storage* **2021**, *40*, 102782. [CrossRef]
187. Kumar, P.M.; Sudarvizhi, D.; Prakash, K.; Anupradeepa, A.; Raj, S.B.; Shanmathi, S.; Sumithra, K.; Surya, S. Investigating a Single Slope Solar Still with a Nano-Phase Change Material. *Mater. Today Proc.* **2021**, *45*, 7922–7925. [CrossRef]
188. Abed, A.H.; Hoshi, H.A.; Jabal, M.H. Experimental Investigation of Modified Solar Still Coupled with High-Frequency Ultrasonic Vaporizer and Phase Change Material Capsules. *Case Stud. Therm. Eng.* **2021**, *28*, 101531. [CrossRef]
189. Elashmawy, M.; Alhadri, M.; Ahmed, M.M.Z. Enhancing Tubular Solar Still Performance Using Novel PCM-Tubes. *Desalination* **2021**, *500*, 114880. [CrossRef]
190. Khalilmoghadam, P.; Rajabi-Ghahnavieh, A.; Shafii, M.B. A Novel Energy Storage System for Latent Heat Recovery in Solar Still Using Phase Change Material and Pulsating Heat Pipe. *Renew. Energy* **2021**, *163*, 2115–2127. [CrossRef]
191. Sonker, V.K.; Singh, R.K.; Chakraborty, J.P.; Sarkar, A. Performance Assessment of a Passive Solar Still Integrated with Thermal Energy Storage and Nanoparticle Stored in Copper Cylinders. *Int. J. Energy Res.* **2021**, *45*, 2856–2869. [CrossRef]
192. Younes, M.M.; Abdullah, A.S.; Essa, F.A.; Omara, Z.M.; Amro, M.I. Enhancing the Wick Solar Still Performance Using Half Barrel and Corrugated Absorbers. *Process Saf. Environ. Prot.* **2021**, *150*, 440–452. [CrossRef]
193. Agrawal, R.; Singh, K.D.P. Performance Evaluation of Double Slope Solar Still Augmented with Binary Eutectic Phase Change Material and Steel Wool Fibre. *Sustain. Energy Technol. Assess.* **2021**, *48*, 101597. [CrossRef]

194. Suraparaju, S.K.; Natarajan, S.K. Experimental Investigation of Single-Basin Solar Still Using Solid Staggered Fins Inserted in Paraffin Wax PCM Bed for Enhancing Productivity. *Environ. Sci. Pollut. Res.* **2021**, *28*, 20330–20343. [CrossRef] [PubMed]
195. Abed, Q.A.; Hachim, D.M. Enhancing the Productivity of Tubular Solar Still by Using the Phase Change Material. *Arab. J. Sci. Eng.* **2021**, *46*, 11645–11660. [CrossRef]
196. Abdelgaied, M.; Zakaria, Y.; Kabeel, A.E.; Essa, F.A. Improving the Tubular Solar Still Performance Using Square and Circular Hollow Fins with Phase Change Materials. *J. Energy Storage* **2021**, *38*, 102564. [CrossRef]
197. Jahanpanah, M.; Sadatinejad, S.J.; Kasaeian, A.; Jahangir, M.H.; Sarrafha, H. Experimental Investigation of the Effects of Low-Temperature Phase Change Material on Single-Slope Solar Still. *Desalination* **2021**, *499*, 114799. [CrossRef]
198. Shoeibi, S.; Kargarsharifabad, H.; Rahbar, N. Effects of Nano-Enhanced Phase Change Material and Nano-Coated on the Performance of Solar Stills. *J. Energy Storage* **2021**, *42*, 103061. [CrossRef]
199. Jaber, H.J.; Rishak, Q.A.; Abed, Q.A. Using PCM, an Experimental Study on Solar Stills Coupled with and without a Parabolic Trough Solar Collector. *Basrah, J. Eng. Sci.* **2021**, *21*, 45–52. [CrossRef]
200. Vigneswaran, V.S.; Kumar, P.G.; Sakthivadivel, D.; Balaji, K.; Meikandan, M.; Dinakar, B.V.; Kamal, K.K.; Kumaresan, G. Energy, Exergy, and Economic Analysis of Low Thermal Conductivity Basin Solar Still Integrated with Phase Change Material for Energy Storage. *J. Energy Storage* **2021**, *34*, 102194. [CrossRef]
201. Parsa, S.M.; Yazdani, A.; Javadi, D.; Afrand, M.; Karimi, N.; Ali, H.M. Selecting Efficient Side of Thermoelectric in Pyramid-Shape Solar Desalination Units Incorporated Phase Change Material (PCM), Nanoparticle, Turbulator with Battery Storage Powered by Photovoltaic. *J. Energy Storage* **2022**, *51*, 104448. [CrossRef]
202. Kumar, S.; Prakash, O. Improving the Single-Slope Solar Still Performance Using Solar Air Heater with Phase Change Materials. *Energies* **2022**, *15*, 8013. [CrossRef]
203. Ho, Z.Y.; Bahar, R.; Koo, C.H. Passive Solar Stills Coupled with Fresnel Lens and Phase Change Material for Sustainable Solar Desalination in the Tropics. *J. Clean. Prod.* **2022**, *334*, 130279. [CrossRef]
204. Moreno, S.; Alvarez, C.; Hinojosa, J.F.; Maytorena, V.M. Numerical Analysis of a Solar Still with Phase Change Material under the Basin. *J. Energy Storage* **2022**, *55*, 105427. [CrossRef]
205. Selimefendigil, F.; Şirin, C.; Öztop, H.F. Experimental Performance Analysis of a Solar Desalination System Modified with Natural Dolomite Powder Integrated Latent Heat Thermal Storage Unit. *Sustainability* **2022**, *14*, 2650. [CrossRef]
206. Ajdari, H.; Ameri, A. Performance Assessment of an Inclined Stepped Solar Still Integrated with PCM and CuO/GO Nanocomposite as a Nanofluid. *J. Build. Eng.* **2022**, *49*, 104090. [CrossRef]
207. Moreno, S.F.; Hinojosa, J.F.; Maytorena, V.M.; Navarro, J.M.A.; Vazquez-Ruiz, A. Thermal Performance and Water Production in a Solar Still With an Energy Storage Material Under Different Concentrations of Salt. *J. Sol. Energy Eng.* **2022**, *145*, 031011. [CrossRef]
208. Maridurai, T.; Rajkumar, S.; Arunkumar, M.; Mohanavel, V.; Arul, K.; Madhesh, D.; Subbiah, R. Performance Study on Phase Change Material Integrated Solar Still Coupled with Solar Collector. *Mater. Today Proc.* **2022**, *59*, 1319–1323. [CrossRef]
209. Hansen, R.S.; Mary, M.B.Q.; Subramanian, S.S.; Raj, J.A.; Gnanaraj, S.J.P.; Appadurai, M. Utilization of PCM in Inclined and Single Basin Solar Stills to Improve the Daily Productivity. *Mater. Today Proc.* **2022**, *62*, 967–972. [CrossRef]
210. Hafs, H.; Ansari, O.; Bah, A. Performance Evaluation of a Production System of Solar Desalination by Using Rectangular Channels with PCM at Different Seasons. *Acta Ecol. Sin.* **2022**, *in press*. [CrossRef]
211. Kuboth, S.; König-Haagen, A.; Brüggemann, D. Numerical Analysis of Shell-and-Tube Type Latent Thermal Energy Storage Performance with Different Arrangements of Circular Fins. *Energies* **2017**, *10*, 274. [CrossRef]
212. Luo, X.; Liao, S. Numerical Study on Melting Heat Transfer in Dendritic Heat Exchangers. *Energies* **2018**, *11*, 2504. [CrossRef]
213. Zarei, M.J.; Bazai, H.; Sharifpur, M.; Mahian, O.; Shabani, B. The Effects of Fin Parameters on the Solidification of PCMs in a Fin-Enhanced Thermal Energy Storage System. *Energies* **2020**, *13*, 198. [CrossRef]
214. Liu, J.; Yu, S.; Yang, S.; Zhang, Y.; Fan, X.; Gao, B. Numerical Studies on the Performance of the PCM Mesh-Finned Heat Sink Base on Thermal-Flow Multiphysics Coupling Simulation. *Energies* **2020**, *13*, 4658. [CrossRef]
215. Pakalka, S.; Valančius, K.; Streckienė, G. Experimental and Theoretical Investigation of the Natural Convection Heat Transfer Coefficient in Phase Change Material (PCM) Based Fin-and-Tube Heat Exchanger. *Energies* **2021**, *14*, 716. [CrossRef]
216. Ghalambaz, M.; Mohammed, H.I.; Mahdi, J.M.; Eisapour, A.H.; Younis, O.; Ghosh, A.; Talebizadehsardari, P.; Yaïci, W. Intensifying the Charging Response of a Phase-Change Material with Twisted Fin Arrays in a Shell-And-Tube Storage System. *Energies* **2021**, *14*, 1619. [CrossRef]
217. Sun, X.; Mahdi, J.M.; Mohammed, H.I.; Majdi, H.S.; Zixiong, W.; Talebizadehsardari, P. Solidification Enhancement in a Triple-Tube Latent Heat Energy Storage System Using Twisted Fins. *Energies* **2021**, *14*, 7179. [CrossRef]
218. Torbarina, F.; Lenic, K.; Trp, A. Computational Model of Shell and Finned Tube Latent Thermal Energy Storage Developed as a New TRNSYS Type. *Energies* **2022**, *15*, 2434. [CrossRef]
219. Chen, Q.; Wu, J.; Sun, K.; Zhang, Y. Numerical Study of Heat Transfer Enhancement by Arc-Shaped Fins in a Shell-Tube Thermal Energy Storage Unit. *Energies* **2022**, *15*, 7799. [CrossRef]
220. Privitera, E.; Caponetto, R.; Matera, F.; Vasta, S. Impact of Geometry on a Thermal-Energy Storage Finned Tube during the Discharging Process. *Energies* **2022**, *15*, 7950. [CrossRef]
221. Yu, M.; Sun, X.; Su, W.; Li, D.; Shen, J.; Zhang, X.; Jiang, L. Investigation on the Melting Performance of a Phase Change Material Based on a Shell-and-Tube Thermal Energy Storage Unit with a Rectangular Fin Configuration. *Energies* **2022**, *15*, 8200. [CrossRef]

222. Liu, J.; Ma, Q.; Li, X. Numerical Simulation of the Combination of Novel Spiral Fin and Phase Change Material for Cylindrical Lithium-Ion Batteries in Passive Thermal Management. *Energies* **2022**, *15*, 8847. [CrossRef]
223. Xu, Y.; Yin, H.; He, C.; Wei, Y.; Cui, M.; Zheng, Z.-J. Structure Optimization of Longitudinal Rectangular Fins to Improve the Melting Performance of Phase Change Materials through Genetic Algorithm. *Energies* **2022**, *15*, 9610. [CrossRef]
224. Rawat, P.; Ashwni; Sherwani, A.F. A Numerical Study on the Impact of Fin Length Arrangement and Material on the Melting of PCM in a Rectangular Enclosure. *Int. J. Heat Mass Transf.* **2023**, *205*, 123932. [CrossRef]
225. Yang, L.; Huang, J.; Zhou, F. Thermophysical Properties and Applications of Nano-Enhanced PCMs: An Update Review. *Energy Convers. Manag.* **2020**, *214*, 112876. [CrossRef]
226. Prabakaran, R.; Sidney, S.; Lal, D.M.; Selvam, C.; Harish, S. Solidification of Graphene-Assisted Phase Change Nanocomposites inside a Sphere for Cold Storage Applications. *Energies* **2019**, *12*, 3473. [CrossRef]
227. Pasupathi, M.K.; Alagar, K.; Mm, M.; Aritra, G. Characterization of Hybrid-Nano/Paraffin Organic Phase Change Material for Thermal Energy Storage Applications in Solar Thermal Systems. *Energies* **2020**, *13*, 5079. [CrossRef]
228. Khan, Z.; Khan, Z.A. Performance Evaluation of Coupled Thermal Enhancement through Novel Wire-Wound Fins Design and Graphene Nano-Platelets in Shell-and-Tube Latent Heat Storage System. *Energies* **2021**, *14*, 3743. [CrossRef]
229. Mohaghegh, M.R.; Tasnim, S.H.; Aliabadi, A.A.; Mahmud, S. Jet Impingement Cooling Enhanced with Nano-Encapsulated PCM. *Energies* **2022**, *15*, 1034. [CrossRef]
230. Zahid, I.; Farooq, M.; Farhan, M.; Usman, M.; Qamar, A.; Imran, M.; Alqahtani, M.A.; Anwar, S.; Sultan, M.; Javaid, M.Y. Thermal Performance Analysis of Various Heat Sinks Based on Alumina NePCM for Passive Cooling of Electronic Components: An Experimental Study. *Energies* **2022**, *15*, 8416. [CrossRef]
231. John, S.; Sreyas, K.; Mohan, Y.; Thampi, A.D.; Rani, S. Numerical Investigation on the Effect of PCM Thickness and Nano-Additive on the Cooling Performance of Stearic Acid Based Battery Thermal Management System. *Mater. Today Proc.* **2023**, *in press*. [CrossRef]
232. Aamer Hayat, M.; Yang, Y.; Li, L.; Bevilacqua, M.; Kang Chen, Y. Preparation and Thermophysical Characterisation Analysis of Potential Nano-Phase Transition Materials for Thermal Energy Storage Applications. *J. Mol. Liq.* **2023**, *376*, 121464. [CrossRef]
233. Aramesh, M.; Shabani, B. Metal Foams Application to Enhance the Thermal Performance of Phase Change Materials: A Review of Experimental Studies to Understand the Mechanisms. *J. Energy Storage* **2022**, *50*, 104650. [CrossRef]
234. Chen, X.; Li, X.; Xia, X.; Sun, C.; Liu, R. Thermal Performance of a PCM-Based Thermal Energy Storage with Metal Foam Enhancement. *Energies* **2019**, *12*, 3275. [CrossRef]
235. Mabrouk, R.; Naji, H.; Dhahri, H.; Younsi, Z. Insight into Foam Pore Effect on Phase Change Process in a Plane Channel under Forced Convection Using the Thermal Lattice Boltzmann Method. *Energies* **2020**, *13*, 3979. [CrossRef]
236. Ghalambaz, M.; Shahabadi, M.; Mehryan, S.A.M.; Sheremet, M.; Younis, O.; Talebizadehsardari, P.; Yaici, W. Latent Heat Thermal Storage of Nano-Enhanced Phase Change Material Filled by Copper Foam with Linear Porosity Variation in Vertical Direction. *Energies* **2021**, *14*, 3979. [CrossRef]
237. Ghalambaz, M.; Mehryan, S.A.M.; Shirivand, H.; Shalbafi, F.; Younis, O.; Inthavong, K.; Ahmadi, G.; Talebizadehsardari, P. Simulation of a Fast-Charging Porous Thermal Energy Storage System Saturated with a Nano-Enhanced Phase Change Material. *Energies* **2021**, *14*, 1508. [CrossRef]
238. Falcone, M.; Rehman, D.; Dongellini, M.; Naldi, C.; Pulvirenti, B.; Morini, G.L. Experimental Investigation on Latent Thermal Energy Storages (LTESs) Based on Pure and Copper-Foam-Loaded PCMs. *Energies* **2022**, *15*, 4894. [CrossRef]
239. Liu, G.; Li, Y.; Wei, P.; Xiao, T.; Meng, X.; Yang, X. Thermo-Economic Assessments on a Heat Storage Tank Filled with Graded Metal Foam. *Energies* **2022**, *15*, 7213. [CrossRef]
240. Hassan, F.; Hussain, A.; Jamil, F.; Arshad, A.; Ali, H.M. Passive Cooling Analysis of an Electronic Chipset Using Nanoparticles and Metal-Foam Composite PCM: An Experimental Study. *Energies* **2022**, *15*, 8746. [CrossRef]
241. Chen, C.; Diao, Y.; Zhao, Y.; Wang, Z.; Liu, Y.; Han, Y.; Zhu, T.; Fang, D.; Li, J. Melting Performance of a Cold Energy Storage Device Filled with Metal Foam–Composite Phase-Change Materials. *J. Energy Storage* **2023**, *60*, 106567. [CrossRef]
242. Sreenath, V.R.; Chanda, S. Thermal Performance Evaluation of PCM-MF Composite Heat Sinks under Varying Ambient Conditions. *Int. J. Heat Mass Transf.* **2023**, *206*, 123927. [CrossRef]